AD-A095 033 NAVAL RESEARCH LAB WASHINGTON DC F/G 4/1
SPREAD F THEORIES - A REVIEW.(U)
JAN 81 S L OSSAKOW
UNCLASSIFIED NRL-MR-4435 NL

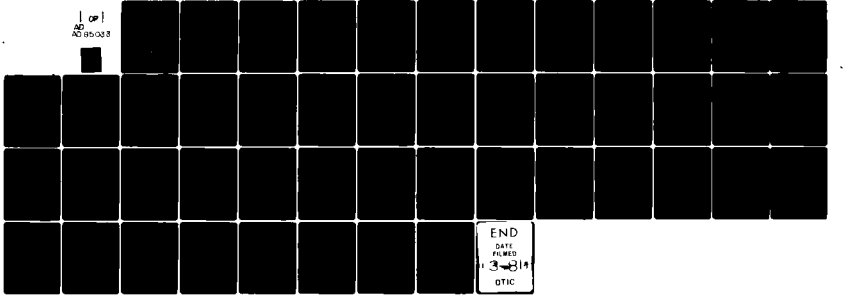

NRL Memorandum Report 4435

Spread F Theories — A Review

S.L. Ossakow

Geophysical and Plasma Dynamics Branch
Plasma Physics Division

January 30, 1981

This research was sponsored partially by the Defense Nuclear Agency under subtask S99QAXHC, work unit title, "Plasma Structure Evolution," and work unit 00002, and partially by the Office of Naval Research.

NAVAL RESEARCH LABORATORY
Washington, D.C.

SECURITY CLASSIFICATION OF THIS PAGE *(When Data Entered)*

REPORT DOCUMENTATION PAGE		READ INSTRUCTIONS BEFORE COMPLETING FORM
1. REPORT NUMBER NRL Memorandum Report 4435	2. GOVT ACCESSION NO. AD-A095 233	3. RECIPIENT'S CATALOG NUMBER
4. TITLE *(and Subtitle)* SPREAD F THEORIES -- A REVIEW*		5. TYPE OF REPORT & PERIOD COVERED Interim report on a continuing NRL problem. 6. PERFORMING ORG. REPORT NUMBER
7. AUTHOR(s) S. L. Ossakow		8. CONTRACT OR GRANT NUMBER(s)
9. PERFORMING ORGANIZATION NAME AND ADDRESS Naval Research Laboratory Washington, DC 20375		10. PROGRAM ELEMENT, PROJECT, TASK AREA & WORK UNIT NUMBERS 61153N; RR0330244; 47-0883-0-1; 62704H; 47-0889-0-1
11. CONTROLLING OFFICE NAME AND ADDRESS Defense Nuclear Agency, Washington, DC 20305 and Office of Naval Research, Arlington, VA 22217		12. REPORT DATE January 30, 1981 13. NUMBER OF PAGES 47
14. MONITORING AGENCY NAME & ADDRESS*(if different from Controlling Office)*		15. SECURITY CLASS. *(of this report)* UNCLASSIFIED 15a. DECLASSIFICATION/DOWNGRADING SCHEDULE

16. DISTRIBUTION STATEMENT *(of this Report)*

Approved for public release; distribution unlimited.

17. DISTRIBUTION STATEMENT *(of the abstract entered in Block 20, if different from Report)*

18. SUPPLEMENTARY NOTES

This research was sponsored partially by the Defense Nuclear Agency under subtask S99QAXHC, work unit title, "Plasma Structure Evolution," and work unit 00002, and partially by the Office of Naval Research.

*This paper is based on an invited review talk given at the Sixth International Symposium on Equatorial Aeronomy, Aguadilla, Puerto Rico, 17–24 July 1980.

19. KEY WORDS *(Continue on reverse side if necessary and identify by block number)*

Equatorial Spread F
Theory
Computer simulation
Review

20. ABSTRACT *(Continue on reverse side if necessary and identify by block number)*

Our understanding of equatorial spread F (ESF) phenomena has progressed significantly in the past several years. ESF phenomena involves ionospheric irregularities spanning some 5-6 orders of magnitude in scale size. The largest scale sizes, on the order of many kilometers, are thought to be caused by a plasma fluid type Rayleigh-Taylor instability mechanism on the bottomside of the nighttime equatorial F region. Plasma density bubbles (depletions) are formed on the bottomside by these ionospheric irregularities and then they rise nonlinearly to the topside, by E X B polarization motion, causing irregularities above the F peak. The power spectral density (PSD) of these long wavelength plasma density fluctuations is proportional to k^{-2}, where k is perpendicular to the geomagnetic field and

(Continues)

DD FORM 1 JAN 73 1473 EDITION OF 1 NOV 65 IS OBSOLETE
S/N 0102-LF-014-6601

SECURITY CLASSIFICATION OF THIS PAGE *(When Data Entered)*

20. Abstract (Continued)

equal to $2\pi/\lambda$. Current theories of the very small scale, $\lesssim$ 10m, radar backscatter observed irregularities (specifically at 3m, 1m, 36 cm, and 11 cm), during ESF, indicate that these irregularities are due to various kinetic type plasma drift wave instabilities. These instabilities are formed by a two step process in which they are driven by the steep plasma density gradients created by the primary long wavelength Rayleigh-Taylor type plasma fluid instabilities. Recent theoretical and numerical simulation studies supporting these ideas on ESF phenomena will be presented.

CONTENTS

SPREAD F THEORIES — A REVIEW

INTRODUCTION

Our understanding of equatorial spread F (ESF) phenomena has increased dramatically over the past few years; notwithstanding the fact that it was discovered over four decades ago (BOOKER and WELLS, 1938) as diffuse echoes on ionograms. Much of this advancement in understanding comes from a combined theoretical and experimental approach to the problem. Advances in radar backscatter measurements, satellite and rocket in situ measurements, and theoretical and numerical simulation techniques have provided a clearer picture of the fundamental mechanisms causing ESF. The study of ESF phenomena has been both complicated and enriched by the fact that the attendant magnetic field aligned ionospheric irregularities span some 5-6 orders of magnitude in scale sizes. The present paper will deal with ESF theory and at that only those theories using plasma mechanisms as a basis. Experimental reviews of the subject can be found in other papers in this edition.

Before we proceed let us examine the basic equatorial nighttime ionospheric F region geometry. Figure 1 depicts this geometry under which ESF occurs. N(y) represents the background zero order electron density as a function of altitude (y). Gravity, $\underline{g}$, points down, the ambient geomagnetic field, $\underline{B}$, is horizontal and pointing north (z), and $\underline{k}$ represents a horizontal perturbation vector and points westward (x). The maximum in the electron density defines the F peak. The bottomside of the profile steepens at night due to chemical recombination effects and upward ambient $\underline{E} \times \underline{B}$ electrodynamic forces. The E region has been reduced by chemical recombination. One might expect this equatorial ionospheric geometry to be unstable to a variety of plasma instabilities because in the plasma physics community fig. 1 represents the classical flute mode geometry.

Manuscript submitted November 5, 1980.

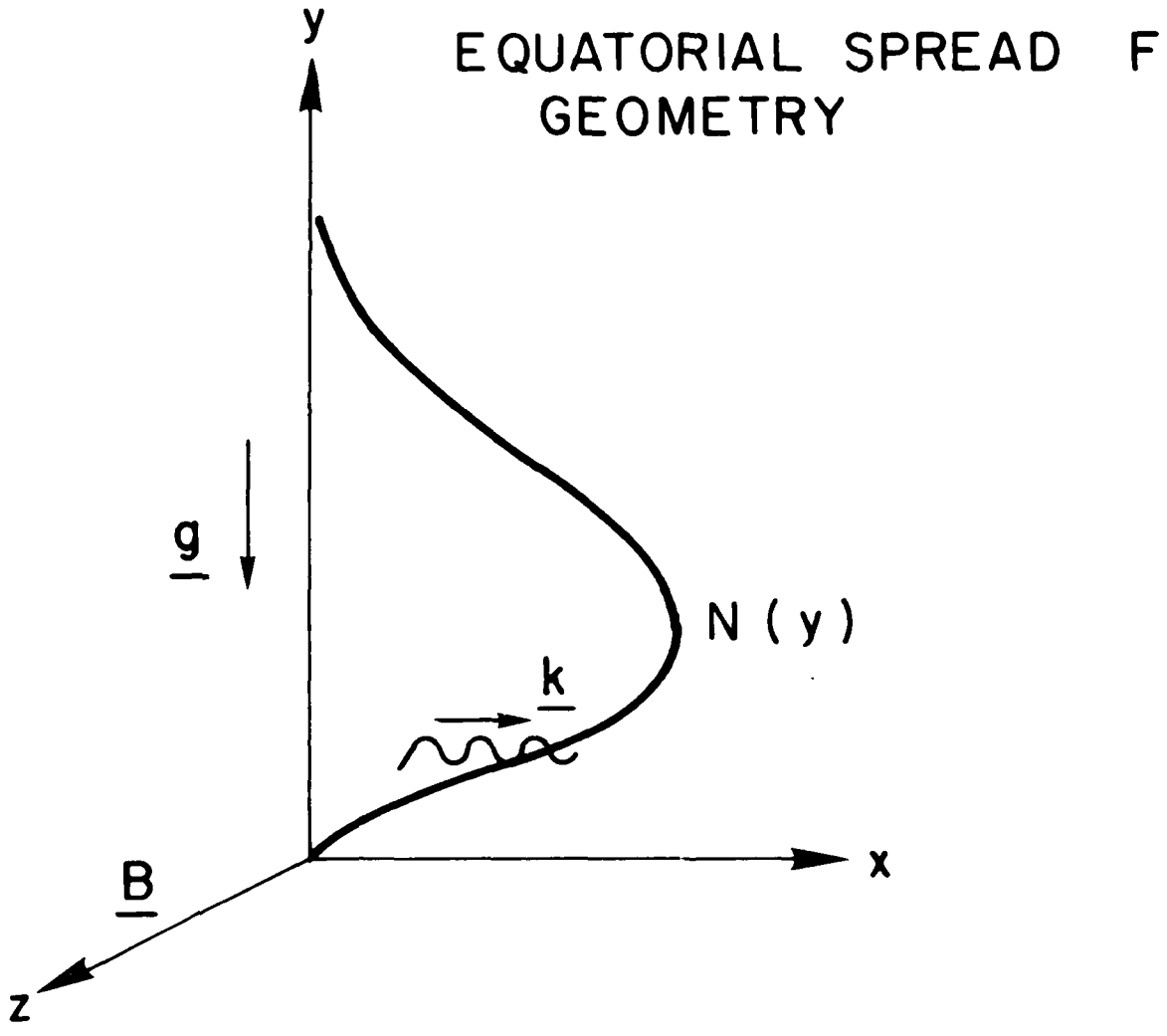

Fig. 1 - Basic equatorial spread F geometry

Notwithstanding the simple geometry exhibited in fig. 1, several basic questions have driven researchers to seek solutions, oftentimes not simple, to the mysteries of ESF phenomena. Some of these basic questions are as follows. (1) Why are plasma density fluctuations observed on both sides of the F peak when linear theory of the representative instabilities predict only bottomside growth (unstable)? (2) Why does the onset of topside spread F lag the onset of bottomside spread F? (3) How are the large plasma depletions (bubbles) produced? (4) What is the power spectrum for the plasma irregularities? (5) What is the relation between the observed backscatter radar short wavelength irregularities and the longer wavelength irregularities observed by in situ measurements and scintillation measurements?

At this juncture, a general brief review will be given of ESF theories. This will be done from an historical perspective, but first we will deal with linear theories and then nonlinear theories. The idea that ESF could be initiated on the bottomside of the F region (see fig. 1) by a Rayleigh-Taylor instability was first proposed by DUNGEY (1956). DAGG (1957) suggested that ESF phenomena was caused by irregularities produced first in the E region and then coupled, by the high conductivity along the magnetic field, up to the F region. It was first suggested by MARTYN (1959) that ESF was a manifestation of the $\underline{E} \times \underline{B}$ gradient drift instability. CALVERT (1963) proposed that the downward motion of the nighttime neutral atmosphere was responsible for ESF. However, this mechanism was essentially equivalent to the $\underline{E} \times \underline{B}$ gradient drift mechanism because of the role played by the relative drift between ions and neutrals in determining the growth rate of the instability. It should be noted that all of the preceding linear instability theories could usually only explain the formation of ESF

irregularities on the bottomside of the F region. These theories were dismissed as inadequate by FARLEY et al. (1970) because they could not explain the wide variety of 3m coherent radar backscatter measurements made at Jicamarca.

In an effort to address the fact that irregularities were observed on both the bottomside and topside of the F region, the collisional Rayleigh-Taylor instability with field line averaging was proposed (BALSLEY et al., 1972; HAERENDEL, 1974). By averaging (integrating) the density along the magnetic field, the total electron content profile becomes steeper on the bottomside of the F region and its peak is raised in altitude with respect to the local electron density peak. Consequently, this allows the linear mechanism to operate to slightly higher altitudes, ~ 100 km greater altitudes, but still would not explain the occurrence of irregularities above this new peak. In the wavelength regime 30m - 100m, HUDSON and KENNEL (1975) pointed out the importance of the collisional drift mode in ESF. This mode had the advantage that it could occur on both the top and bottomside of the F region, but still would not explain the longer wavelength irregularities. Finite larmor radius (FLR) corrections were also applied to the collisionless and collisional Rayleigh-Taylor instability in their work. These FLR effects had more of a stabilizing influence, at short wavelengths, on the collisionless rather than the collisional regime. CHIU and STRAUS (1979) reexamined the linear theory of the Rayleigh-Taylor instability in the nighttime equatorial ionosphere, in the 100 km to the bottomside F region altitude range. They included (a) the eastward drift of the ionosphere caused by the nighttime polarization electric field; (b) the eastward nighttime neutral wind; and (c) recombination in the E and F regions. They found that, well below the bottomside F region, the Rayleigh-Taylor mode

could be unstable, being driven by an eastward neutral wind (with the plasma density gradient in altitude) rather than by gravity. This investigation dealt with instability only below the F peak.

Because of the inability of linear theory to explain most ESF phenomena, several nonlinear theories have been set forth in an attempt to explain the various observations. HAERENDEL (1972; 1974) was the first to suggest that the range of wavelengths (many kilometers down to centimeters) observed during ESF was due to a hierarchy of (multi-step) processes. The picture portrayed was as follows: (i) the collisional Rayleigh-Taylor (R-T) instability with horizontal wavevectors is driven by gravity and the vertical background, zero order electron density gradient scale length on the bottomside (see fig. 1); then (ii) the $\underline{E} \times \underline{B}$ gradient drift instability with vertical wavevectors arises due to the horizontal density, large amplitude variations (with shorter scale lengths than the original zero order vertical density gradient) set up by the collisional R-T instability; then (iii) the inertia (collisionless) dominated R-T instability arises; and finally (iv) kinetic drift waves grow off these irregularities after they reach large amplitude. Because each succeeding process is driven by smaller and smaller plasma density gradient scale lengths, all scale size irregularities will appear almost simultaneously.

In the same spirit, HUDSON, et al. (1973) suggested that the very smallest scale ($\lesssim$ 10m) irregularities, i.e., those observed by coherent backscatter radar techniques, were due to a two step process. In this prescription a long wavelength collisional drift mode grows on the zero order vertical density gradient to finite amplitudes, generating horizontal density gradients. These horizontal gradients in turn generate an unstable kinetic short wavelength drift mode at wavelengths less than the ion gyroradius.

CHATURVEDI and KAW (1975a,b) have examined the formation of steady-state ESF irregularities in the collisionless R-T regime, using a nonlinear one-dimensional set of equations to describe the instability. CHATURVEDI and KAW (1976) interpreted the k^{-2} (where k is the wavenumber perpendicular to the geomagnetic field and equal to $2\pi/\lambda$ and λ is the wavelength) measured power spectrum of the ESF plasma density irregularities in terms of a two step theory. In this particular theory longer wavelength R-T modes couple to kinetic collisional drift waves in such a manner that the mode coupling results in the observed k^{-2} spectrum.

SCANNAPIECO and OSSAKOW (1976) performed the first numerical simulation of the long wavelength collisional R-T instability mechanism in the nighttime equatorial F region ionosphere. The simulation was two dimensional (x,y see fig. 1) in the plane perpendicular to the ambient geomagnetic field, using only gravity and the vertical plasma density gradient (with an actual ionospheric electron density profile) as drivers of the instability. The simulation results showed that the collisional R-T instability generated irregularities and plasma bubbles (plasma density depletions) on the bottomside of the nighttime F region which then rose beyond the F peak by nonlinear polarization induced $\underline{E} \times \underline{B}$ motion. This was a major breakthrough as it represented the first theoretical result to explain how long wavelength irregularities could appear on both the bottomside and topside of the equatorial F region. The bubble phenomena was in accord with many observations (KELLEY et al., 1976; WOODMAN and LA HOZ, 1976; McCLURE et al., 1977). An analytic nonlinear mode-mode coupling theory for the coherent development of the collisional R-T instability was performed by CHATURVEDI and OSSAKOW (1977). In this theory linearly unstable collisional R-T modes in the x-y plane (see fig. 1) saturate nonlinearly by exciting linearly damped vertical

modes, i.e., these vertical modes rise nonlinearly to large amplitudes. In addition, the theory suggested that the vertical modes would be dominant and result in a k^{-2} power spectrum. HUDSON (1978) extended the results of CHATURVEDI and OSSAKOW (1977) to the collisionless R-T regime and reached similar conclusions.

Given the observational and numerical simulation evidence for ESF bubbles, some theoretical research has been directed towards bubble phenomenology in the ESF ionosphere. Analytical models for the rise of ESF bubbles in the collisional and collisionless R-T regime, in analogy with fluid bubbles, were given by OTT (1978). The result of his study predicts the bubbles to be cylindrical (circular cap at the top) in the two dimensions perpendicular to $\underline{B}$. In the collision dominated R-T regime, for a 100% depletion, the bubble rise velocity $V_B = g/\nu_{in}$, where ν_{in} is the ion-neutral collision frequency and g is gravity. In the collisionless or inertia dominated R-T regime, for a 100% depletion, the bubble rise velocity turns out to be $V_B \approx (Rg)^{\frac{1}{2}}/2$, where R is the radius of curvature at the top of the bubble so that this velocity becomes bubble size dependent. OSSAKOW and CHATURVEDI (1978) have presented two dimensional (in plane perpendicular to $\underline{B}$), analytic models for the rise of ESF bubbles in the collisional R-T regime, within the framework of the electrical analogy with barium clouds. Different bubble geometries were investigated with the results of all studies expressible as $V_B = (g/\nu_{in})\ f(\delta n/n_o)$, where $f(\delta n/n_o)$ is an increasing function of the percentage depletion $\delta n/n_o$ (with the case of a 100% cylindrical depletion being g/ν_{in}). SZUSZCZEWICZ (1978) has discussed the chemistry and transport of ESF bubbles. Investigation of vertical induced $\underline{E} \times \underline{B}$ ESF bubble motion, incorporating flux tube integrated quantities of electron content and Pedersen conductivity, has been carried out by ANDERSON and HAERENDEL (1979).

The slab model that they used for the bubble resulted in a simple expression for the induced electric field in the east-west direction. The calculations showed that the vertical bubble rise velocity as a function of time critically depended on the background electric field. Recently, BURKE (1979) has investigated the physical properties of ESF bubbles in the topside F region ionosphere near the dawn terminator. The study deals with the effects of the E region after sunrise in discharging the electric fields within the bubbles. The results show that the conducting E region can effectively halt the upward bubble rise velocity.

COSTA and KELLEY (1978a;b) suggested that coherent steepened structures and not turbulence would give a k^{-2} power spectrum for ESF irregularities. Furthermore, these sharp plasma density gradients could cause small scale sizes ($\sim$ 20m) by collisionless low frequency ($\ll$ ion gyrofrequency, ω_i) kinetic drift waves through a two step process. This idea was set forth to explain the 3m Jicamarca radar observed irregularities. This analysis and subsequent ones (HUBA et al., 1978; HUBA and OSSAKOW, 1979a;b; 1980) to explain the coherent backscatter radar observed irregularities are really linear calculations in the following sense. The steepened gradients are formed by nonlinear evolution of a primary instability, e.g., R-T, and then one performs a linear theory, for a secondary instability (e.g., kinetic drift wave), using the nonlinear state plasma density gradient as a driver. Inclusion of electron-ion, electron-neutral, and ion-ion collisions by HUBA and OSSAKOW (1979a) into the low frequency drift wave theory invoked by COSTA and KELLEY (1978b) showed that linear theory could not explain the 3m irregularities. Rather one could get down to only about 10m with these low frequency drift waves (with collisions).

HUBA et al. (1978) reported on very small scale (1m and 36 cm) ESF irregularities which were experimentally observed by coherent radar backscatter techniques at Kwajalein. A two step process, utilizing high frequency ($\geq \Omega_i$) kinetic drift cyclotron (DC) or lower hybrid drift (LHD) instabilities was invoked to explain these irregularities below the ion gyroradius. This linear instability analysis, including ion-ion collisions, performed on a nonlinear state, favored the formation of LHD instabilities. The results provided an encouraging explanation of the very short wavelengths. More detailed analyses including various collisional effects have been performed on the high frequency drift waves in these inhomogeneous plasmas. HUBA and OSSAKOW (1979b) showed how cyclotron resonances could be destroyed in weakly collisional inhomogeneous plasmas. Ion-ion and electron-electron collisions were considered and the results showed how the DC instability went into the LHD instability. SPERLING and GOLDMAN (1980) looked further into electron collisional effects on the LHD instability. They originally included both electron-ion and electron-neutral collisions, but in their final analysis only showed the effects of electron-ion collisions. The work of HUBA and OSSAKOW (1980) included electron-neutral as well as electron-ion collisions in their LHD instability explanation of 11 cm irregularities observed at high altitudes ($\sim$ 500 km) during ESF conditions at Kwajalein. The absence of these irregularities at lower altitudes was attributed to the stabilizing influence of electron-neutral collisions. All of the short wavelength (1m, 36 cm, and 11 cm) irregularities observed at Kwajalein during ESF appear to be explainable (for initiation purposes) by the linear theory of the LHD instability in the condition favoring low plasma densities and steep plasma density gradients. However, the region encompassing greater than one meter to about 10m seems to be inaccessible to either

the linear theory of the low frequency or high frequency kinetic instabilities mentioned above, for reasonable plasma density gradients.

KELLEY and OTT (1978) have proposed that the ESF bubbles, in the collisionless R-T regime, generate a wake with vortices. Two dimensional fluid turbulence theory was then applied to the model. This resulted in the development of turbulence at shorter and longer wavelengths than the bubble size. This in turn led to a prediction of k^{-1} for the power spectrum of ESF irregularities (which does not appear to be in agreement with experimental observations which favors k^{-2}) in the range $L_S^{-1} < k < L_D^{-1}$, where L_S is the stirring (bubble) size and L_D is a dissipation length cutoff.

OSSAKOW et al. (1979) extended the earlier numerical simulation work of SCANNAPIECO and OSSAKOW (1976) on nonlinear ESF to study the dependence on altitude of the F peak and bottomside background electron density gradient scale length. It was found that under favorable conditions, i.e., high altitude of the F peak and/or steep bottomside background electron density gradients, the collisional R-T instability caused linear growth on the bottomside of the F region. Subsequently, this caused plasma bubbles (density depletions) to be formed on the bottomside which then steepened on their top and rose nonlinearly above the F peak by polarization $\underline{E} \times \underline{B}$ motion. While rising the bubbles elongated in the altitude direction. This sequence of events produced irregularities on the topside of the F region where linear theory of the collisional R-T instability would predict no irregularities (stability). High altitude of the F peak, small bottomside background electron density gradient scale lengths, and large initial bottomside percentage depletions yielded large vertical bubble rise velocities. Changing the altitude of the F peak (e.g., raising it 80 km above the case of SCANNAPIECO and OSSAKOW (1976)) exhibited dramatic effects on ESF evolution.

The higher rise velocities due to the elevated F peak produced results in good agreement with the high velocity measurements of KELLEY et al. (1976) and McCLURE et al. (1977).

Further numerical simulations (ZALESAK and OSSAKOW, 1980) in the collisional R-T regime have shown that horizontally large spatial ESF bubbles ($\sim$ 50-100 km wide), with almost 100% depletions (several orders of magnitude change in plasma density) and large rise velocities, can be produced with an initially long wavelength plasma density perturbation. The evolution of such bubbles is on the same time scale as the small scale bubbles studied by OSSAKOW et al. (1979), but the plasma comes from lower altitudes in the equatorial ionosphere. This last fact is a consequence of the greater penetration of the polarization fringe field into the lower ionosphere in the large versus the small bubble case (see next theory section). KESKINEN et al. (1980) have performed nonlinear numerical simulations of the intermediate wavelength (100m - 1 km) collisional R-T instability in local unstable regions of the postsunset bottomside ($\sim$ 300 km altitude) equatorial F region ionosphere. It is found that the linearly unstable modes saturate by nonlinear excitation of linearly damped vertical modes. In addition, the one dimensional power spectrum for these irregularities in both the horizontal and vertical directions is $\propto k^{-n}$, where n = 2-2.5. These results support the nonlinear analytic studies of CHATURVEDI and OSSAKOW (1977). Preliminary numerical simulations have been performed (CHATURVEDI et al., 1978) in the collisional R-T regime in which an eastward neutral wind (relative to the plasma motion) was added. These results indicated that the wind caused a vertical polarization electric field which in turn caused the ESF bubbles to move westward with respect to the plasma in agreement with the observations of McCLURE et al. (1977). The need of an eastward neutral wind to produce

the westward drift of the rising bubbles had been hypothesized by WOODMAN and LA HOZ (1976), OTT (1978) and OSSAKOW and CHATURVEDI (1978).

Much work and significant progress in the theoretical area of ESF phenomena has been accomplished in the past few years. In spite of the success further work still needs to be done (these areas are summarized in the last section of this paper). Theoretical and numerical simulation efforts are continuing. The next section briefly presents some of the representative theoretical efforts mentioned in the preceding paragraphs. The final section presents a summary concerning ESF theory and remaining problem areas.

THEORY

In this section we present some representative theoretical and numerical simulation works with the appropriate references.

General

The basic plasma fluid equations applicable to the ESF ionosphere are as follows:

$$\frac{\partial n_\alpha}{\partial t} + \nabla \cdot (n_\alpha \underline{V}_\alpha) = P - \nu_R n_\alpha \tag{1}$$

$$-T_e \nabla n_e - e n_e \left(\underline{E} + \frac{\underline{V}_e \times \underline{B}}{c}\right) = 0 \tag{2}$$

$$m_i n_i \left(\frac{\partial}{\partial t} + \underline{V}_i \cdot \nabla\right)\underline{V}_i = -T_i \nabla n_i + e n_i \left(\underline{E} + \frac{\underline{V}_i \times \underline{B}}{c}\right) + m_i n_i \underline{g} - m_i n_i \nu_{in} \underline{V}_i \tag{3}$$

$$\nabla \cdot \underline{J} = 0 \tag{4}$$

$$\underline{J} = ne(\underline{V}_i - \underline{V}_e) \tag{5}$$

In the above equations the subscript α denotes species (e is electron, i is ion), n is density, $\underline{V}$ is velocity, P is the production, ν_R is the chemical recombination coefficient, T is temperature, ∇ is the gradient operator, $\underline{B}$ is the ambient magnetic field (taken to be uniform), e is the electronic charge, c is the speed of light, m is mass, $\underline{g}$ is gravity, ν_{in} is the ion-neutral collision frequency, and $\underline{J}$ is current. In addition, we have neglected neutral wind effects. Equation (1) is the continuity equation, (2) and (3) are the electron and ion momentum equations, respectively, (4) is the divergence of the current and (5) is the current equation. What we have in mind is to apply the set of equations (1) - (5) to the two dimensions perpendicular to $\underline{B}$ at the geomagnetic equator, making various approximations.

If inertial terms are neglected (i.e., the left hand side of (3)), we take $\nu_{in}/\Omega_i \ll 1$ (valid in the F region), and we make the quasi-neutral approximation, $n_e \approx n_i \approx n$, then (1) - (3) become for the two dimensions (x,y) perpendicular to $\underline{B}$

$$\frac{\partial n_\alpha}{\partial t} + \nabla \cdot (n_\alpha \underline{V}_\alpha) = - \nu_R \, n_\alpha \tag{6}$$

$$\underline{V}_e = \frac{c}{B} \underline{E} \times \hat{z} \tag{7}$$

$$\underline{V}_i = \left(\frac{\underline{g}}{\Omega_i} + \frac{c}{B} \underline{E} \right) \times \hat{z} + \frac{\nu_{in}}{\Omega_i} \frac{\underline{g}}{\Omega_i} + \frac{c}{B} \underline{E} \tag{8}$$

where $\Omega_i = eB/m_i c$, $\underline{B} = B\hat{z}$ and we have set $T_e = T_i = 0$ for simplicity (see OSSAKOW et al., 1979). We have neglected the $\underline{g} \times \hat{z}$ motion in (7) because compared with the same ion motion it is in the ratio m_e/m_i. Making the electrostatic approximation $\underline{E} = - \nabla\phi$ and setting $\phi = \phi_o + \tilde{\phi}$, where the subscript zero refers to equilibrium or zero order quantities and the tilde refers to perturbed quantities, we obtain

$$\frac{\partial n}{\partial t} - \frac{c}{B} (\nabla\tilde{\phi} \times \hat{z}) \cdot \nabla n = - \nu_R n \tag{9}$$

$$\nabla \cdot (\nu_{in} n \nabla\tilde{\phi}) = \frac{B}{c} (\underline{g} \times \hat{z}) \cdot \nabla n \tag{10}$$

In arriving at (10) we have put (7) and (8) into (4) and (5) and obtained $\nabla\phi_o = m_i \underline{g}/e$. Equation (9) is the electron continuity equation in the $- \nabla\phi_o \times \underline{B}$ drift frame (i.e., $- \underline{g} \times \hat{z}/\Omega_i$ frame).

To obtain a linear growth rate from (9) and (10) we set $n = n_o(y) + \tilde{n}$ and put $\tilde{n}$, $\tilde{\phi} \propto \exp i(\underline{k}_\perp \cdot \underline{x} - \omega t)$ where $k_\perp^2 = k_x^2 + k_y^2$ and $\omega \equiv \omega_r + i\gamma$. The growth rate γ then is, for $k_\perp L \gg 1$,

$$\gamma = \frac{g}{\nu_{in} L} \left(\frac{k_x}{k_\perp}\right)^2 - \nu_R \; ; \; L^{-1} \equiv \frac{1}{n_o} \frac{\partial n_o}{\partial y} \tag{11}$$

For horizontal waves, i.e., $k_\perp = k_x$ this reduces to

$$\gamma = \frac{g}{\nu_{in} L} - \nu_R \tag{12}$$

Equations (11) and (12) represent the linear growth rate in the collisional R-T regime. Linearizing the more general set of equations (1) - (5), with ion inertial terms, would have resulted in the growth rate

$$\gamma = \frac{\left[-\nu_{in} + (\nu_{in}^2 + 4gL)^{1/2}\right]}{2} - \nu_R \tag{13}$$

which reduces to

$$\gamma = \begin{cases} \dfrac{g}{\nu_{in} L} - \nu_R & \text{for } \nu_{in}^2 \gg 4g/L \qquad (14a) \\ \left(\dfrac{g}{L}\right)^{1/2} - \nu_R & \text{for } \nu_{in}^2 \ll 4g/L \qquad (14b) \end{cases}$$

Equation (14a) is just (12) and (14b) represents the collisionless (inertia dominated) R-T regime.

2D Global Numerical Simulation Results

In this section we will outline some two dimensional ($\perp\underset{\sim}{B}$) numerical simulation results of the collisional R-T instability mechanism (ZALESAK and OSSAKOW, 1980). The simulation plane encompasses an altitude extent of over 200 km, from the bottomside to topside of the ESF region. Ionospheric profiles of $n_o(y)$, $\nu_{in}(y)$, and $\nu_R(y)$ are used in the simulations (see figs. 2 and 3). A simulation mesh of 140 (altitude, y) by 40 (east-west, x) was employed with Δy = 2 km and Δx = 5 km (large case, L) and Δx = 200m (small case, S). The boundary conditions were periodic in x and in y transmittive for n and Neumann for the induced potential, $\tilde{\phi}$. Equations (9) and (10) were utilized, with n_o obeying $\partial n_o/\partial t = -\nu_R n_o$. Two different types of initial perturbations and different wavelengths corresponding to the large case and small case were used (4 cases in all). However, here we will only present cases 1S and 1L which are defined with Δx = 200m and Δx = 5 km, respectively, and a perturbation of the form (see ZALESAK and OSSAKOW, 1980 for more details)

$$\frac{n(x,y,0)}{n_o(y,0)} = 1 - e^{-3}\cos\left(\frac{\pi x}{8\Delta x}\right) \quad 0 \le |x| \le 8\Delta x$$

$$\frac{n(x,y,0)}{n_o(y,0)} = 1 - e^{-3}\,\frac{1}{2}\left[\cos\left(\frac{\pi x}{8\Delta x}\right) - 1\right] \quad 8\Delta x \le |x| \le 16\Delta x$$

$$\frac{n(x,y,0)}{n_o(y,0)} = 1 \quad |x| > 16\Delta x \qquad (15)$$

In contrast to this more localized type of perturbation which has been used before (OSSAKOW et al., 1979) the pure sinusoidal one, also used by ZALESAK and OSSAKOW (1980), will not be shown here.

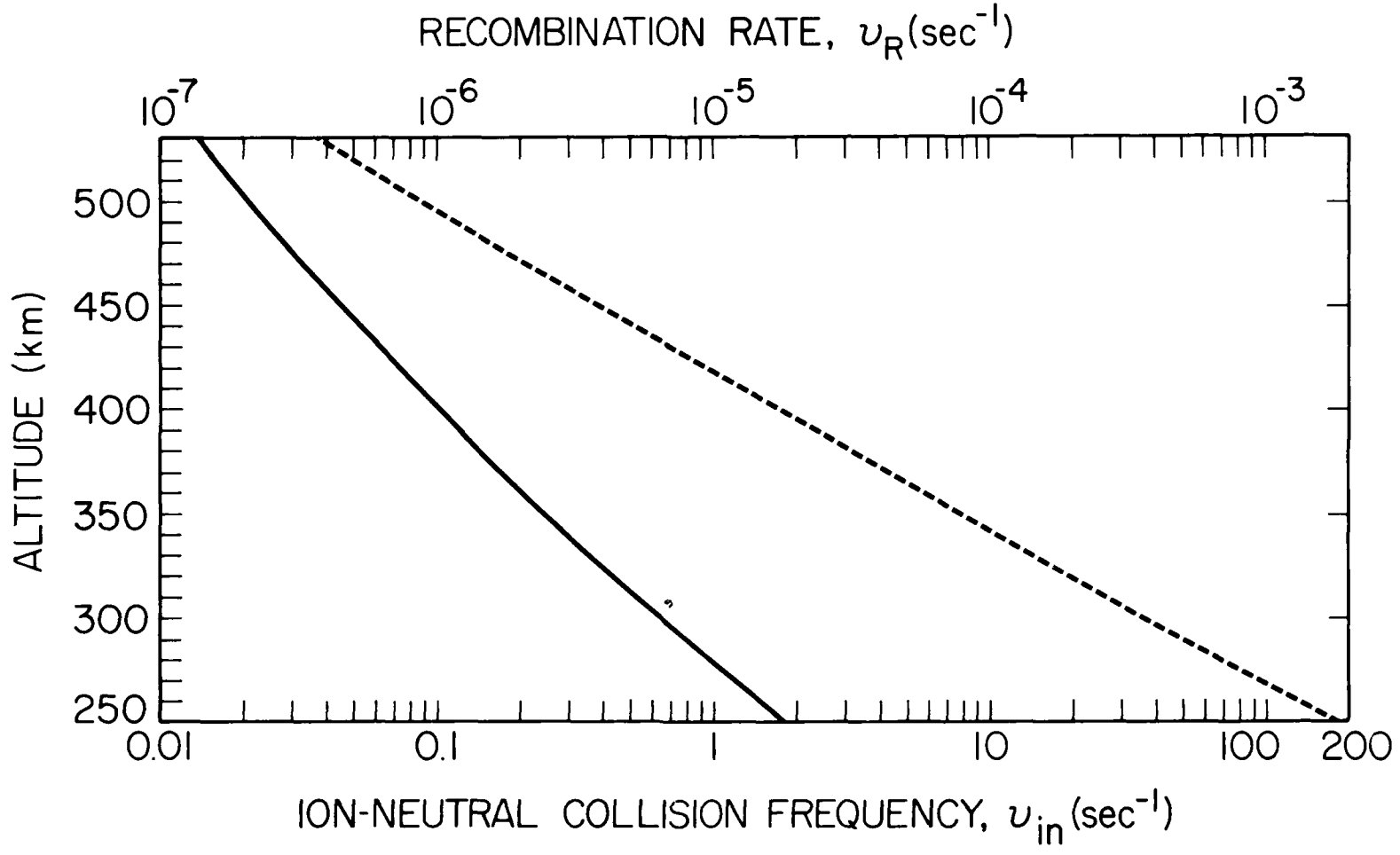

Fig. 2 - The ion-neutral collision frequency, ν_{in} (solid), and recombination coefficient (rate), ν_R (dashed), as a function of altitude used in the numerical simulations (after ZALESAK and OSSAKOW, 1980).

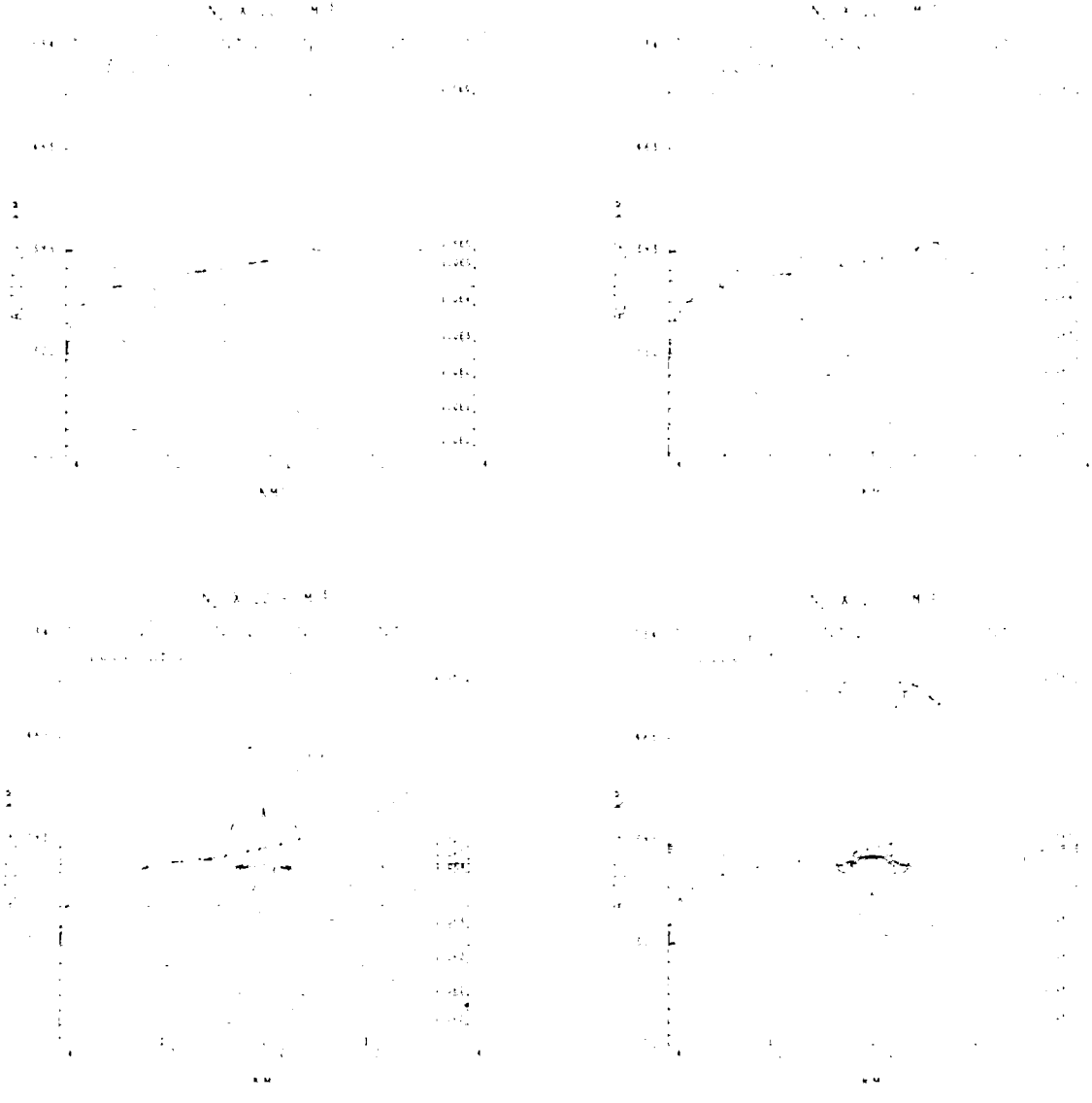

Fig. 3 - Sequence of four plots showing isoelectron density contours of calculation 1S at 300, 700, and 1000, and 1200 sec. Superimposed on each plot is a dashed line showing n_o (y,t) and labeled at the top. Electron densities are given in cm^{-3}. The observer is looking southward so that $\underline{B}$ is out of the figure (after ZALESAK and OSSAKOW, 1980).

Figures 3 and 4 are a comparison of small versus large horizontal extent. Figure 2 shows isodensity contours of calculation 1S at times 300, 700, 1000, and 1200 seconds after initialization. Figure 3 shows the same contours at the same times but for calculation 1L. The presence of much lower density plasma fluid in the bubble in calculation 1L is obvious. There is also a basic difference in bubble morphology at late times. At 1200 seconds, 1S has pinched off into two bubbles, with the more intense one below the initial central bubble. In addition, another bubble has formed in the sides of the computational mesh. These structures are more obvious in the plot of $n(x,y)/n_o(y)$ at 1200 seconds for 1S shown in fig. 5a. The maximum depletion levels are 70% in the top central bubble, 97% in the lower central bubble, and 95% in the side bubble. In the lower bubble in fig. 4a the outermost contour has $n/n_o = 0.5$ (50% depletion) and the innermost, fifth contour has $n/n_o = 0.03$ (97% depletion). In obtaining percentage enhancements and depletions one subtracts 1.0 from n/n_o.

The results of calculation 1L, in figs. 3 and 4, show a single plume of depleted ionization at 1200 seconds, with no secondary central bubble or side bubble. In fig. 5b a plot of $n(x,y)/n_o(y)$ for case 1L at 1200 seconds is exhibited. The level of depletion is greater than 99.9% for the entire 10 km by 70 km oval hole located inside the tenth solid contour of fig. 5b and represents at least a three ordersof magnitude decrease (bite-out) in plasma density. The bubble rise velocity for each case, computed from the last two frames of figs. 2 and 3, are 1S = 210 m/s and 1L = 230 m/s. These large bite-outs and large rise velocities are in agreement with the observations of McCLURE et al., (1977).

The reason that the bubble is more depleted in the 1L case versus the 1S case (see figs. 3, 4 and 5) can be seen with the aid of fig. 6, which

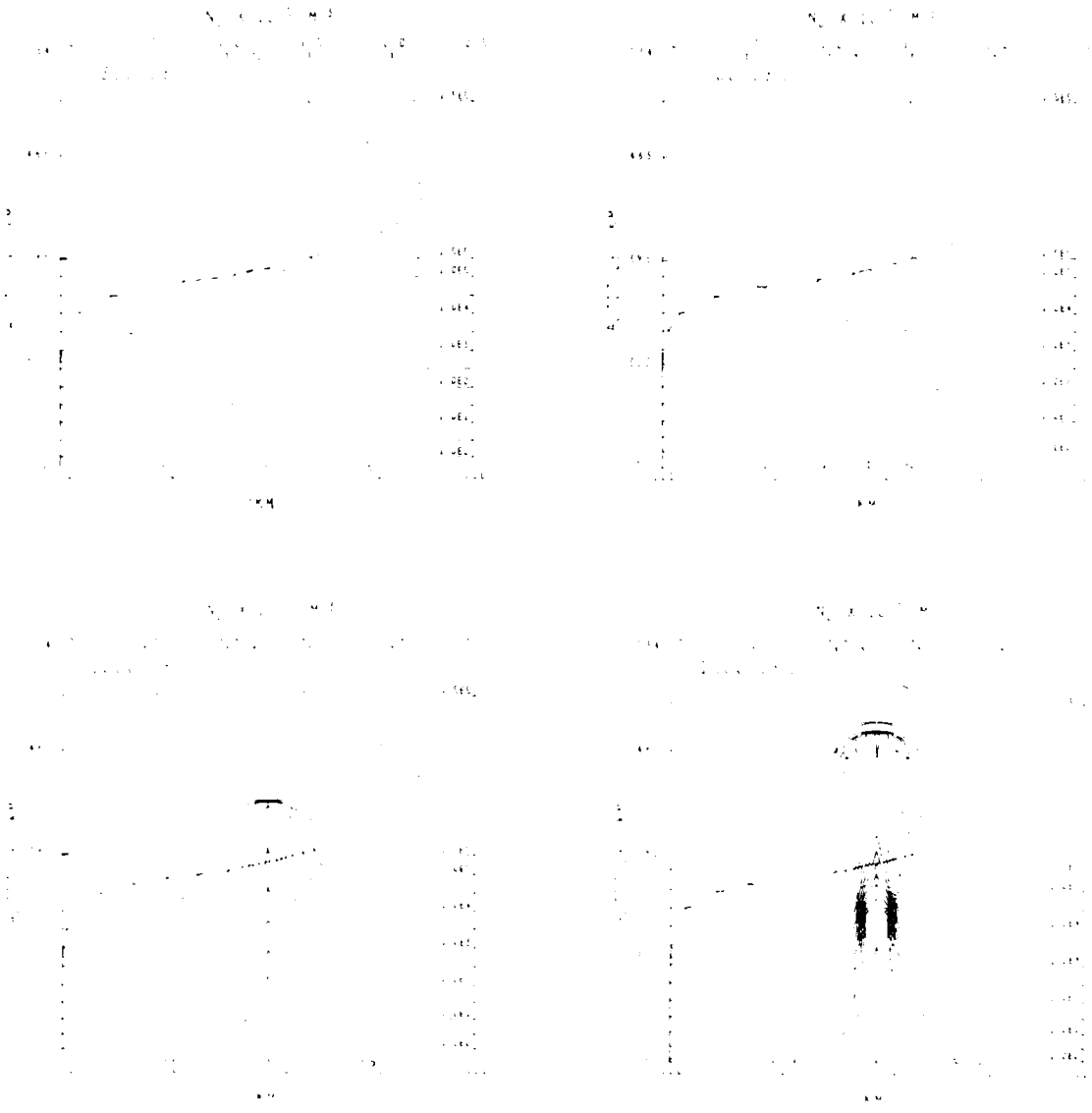

Fig. 4 - Same as figure 3 but for calculation 1L (after ZALESAK and OSSAKOW, 1980)

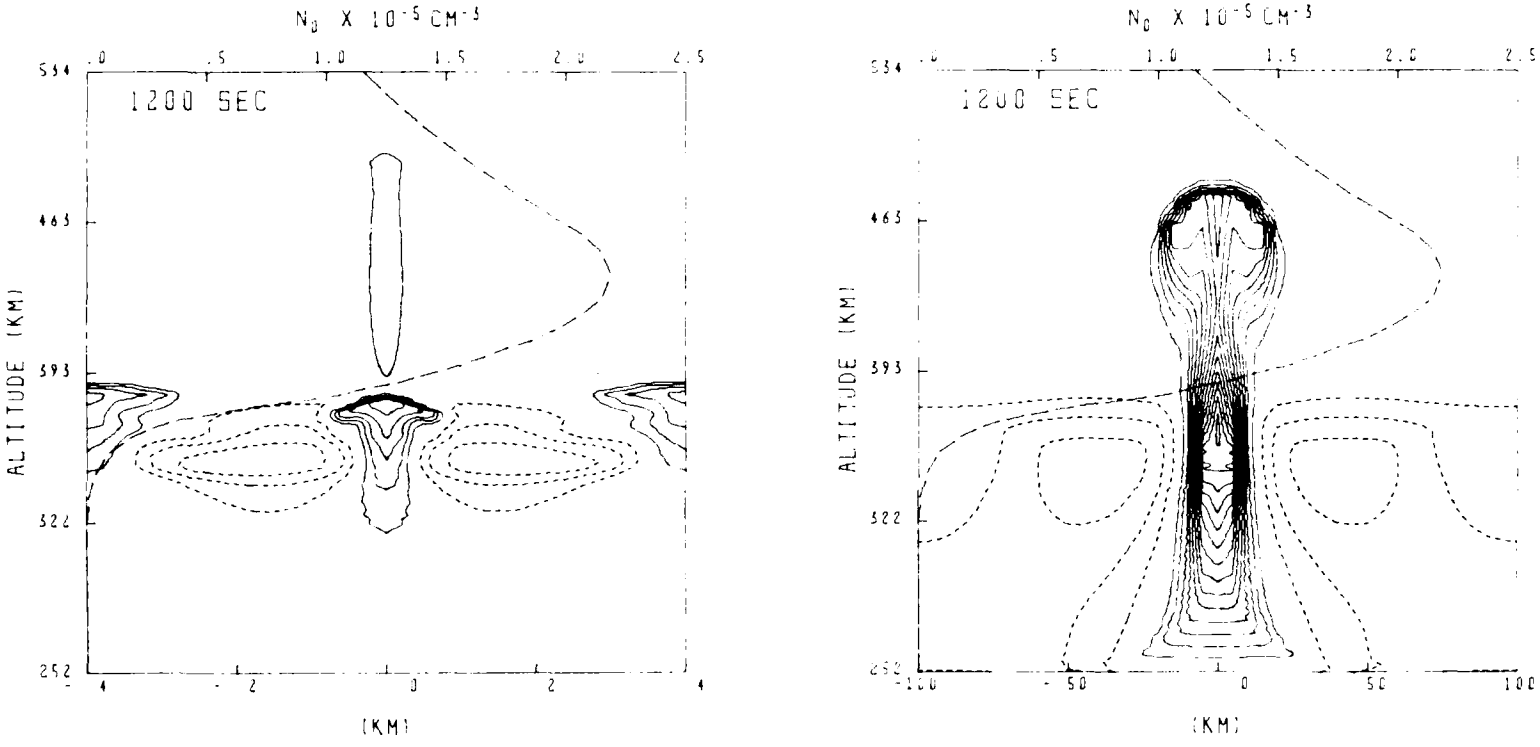

Fig. 5 - Contours of constant $n(x,y,t)/n_o(y,t)$ for (a) 1S at 1200 s and (b) 1L at 1200 s. Depletions ($n/n_o < 1$) are shown in solid lines, while enhancements ($n/n_o > 1$) are shown as short dashed lines. The first (outermost) depletion contour is for $n/n_o = 0.5$, while each succeeding contour is for a value of n/n_o, a factor of 0.5 times the previous one. The first enhancement contour is for $n/n_o = 2.0$, while each succeeding contour is for a value of n/n_o, a factor of 2.0 times the previous one. The superimposed long dashed line depicts $n_o(y,t)$ (after ZÅLESAK and OSSAKOW, 1980).

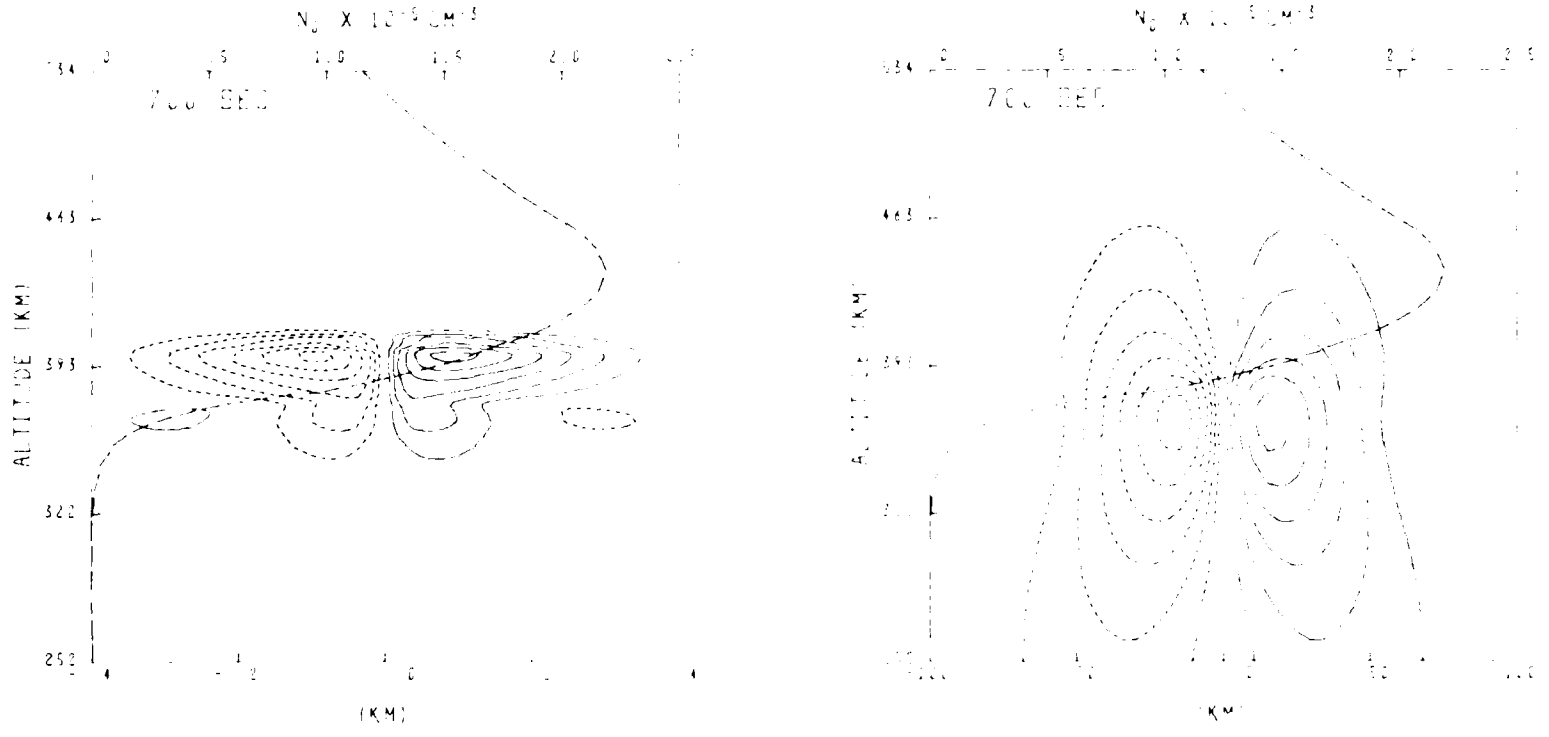

(a) (b)

Fig. 6 - Contours of constant induced electrostatic potential at 700 s. for (a) calculation 1S and (b) calculation 1L. Small dashed lines are for negative potentials and solid lines are for positive potentials. The potential drop across adjacent contours is a constant in each plot except that the zero potential is not plotted. In each case the contours are chosen to space the twelve contours (plus the zero contour) uniformly from maximum to minimum potential. The large dashed line depicts $n_o(y)$ at 700 s. (after ZALESAK and OSSAKOW, 1980).

shows the induced electrostatic potential, $\tilde{\Phi}$, at 700 seconds. Notice that the fringe field surrounding the bubble in the IL case extends to lower altitudes than in the IS case. Since the contours of constant potential are in fact flow streamlines, more plasma from lower altitudes is being drawn upward in the IL case than in the IS case. The effect is similar to the fringe field of a parallel plate capacitor. In that case the distance outside the plates that the electric field goes is proportional to the plate separation. In the case depicted in fig. 6 the role of plate separation is played by the horizontal size of the bubble (see ZALESAK and OSSAKOW, 1980 for more details).

The results gleaned from these numerical simulations of large horizontal wavelength initial perturbations in the collisional R-T regime are as follows. The large scale length initial perturbations evolve nonlinearly into large horizontal scale length ESF bubbles. These bubbles evolve approximately on the same time scale as do the smaller horizontal scale length counterparts. The plasma comprising these large bubbles has its origin at much lower altitudes than that of the smaller horizontal scale lengths bubbles and this results in plasma density depletions in the large bubbles very close to 100%, i.e., several orders of magnitude depletions.

Local Numerical Simulations

In this section we will show an example of some computer simulations of intermediate wavelength ($\sim$ 100m - 1 km) collisional R-T instability evolution in local unstable regions of the postsunset bottomside ($\sim$ 300 km altitude) equatorial F region ionosphere (KESKINEN et al., 1980). These simulations are called local compared with the ones presented in the previous section in the sense that a chunk of the F region is looked at with a more finely resolved computational mesh. The price one pays, of course, is that one

cannot cover a great altitude or east-west extent and still resolve shorter wavelengths (remember the ESF associated irregularity phenomena cover some 5-6 orders of magnitude in scale size). In these particular simulations a 64 by 64 computational mesh in the plane perpendicular (x,y) to $\underline{B}$ is utilized with $\Delta x = \Delta y = 15m$ (so we basically have a 1 km by 1 km chunk). Simulations have been run for ambient bottomside electron density gradient scale lengths L = 5, 10, and 15 km (where we have taken $n_o(y) = N_o(1 + (y/L))$. Bottomside ionospheric parameters corresponding to an altitude of 300 km has been used.

With the above ideas in mind, equations (9) and (10) have been used, except that a term $\nu_R n_o$ has been added to the right side of (9). If one sets $n = n_o$ in (9) this shows that $\partial n_o/\partial t = 0$, i.e., n_o is taken not to change. In addition, the simulations were initialized with a two dimensional perturbation of the following form

$$\frac{\tilde{n}(x,y,t = 0)}{n_o} = A_{1,1} \sin k_x x \cos k_y y + A_{2,0} \sin 2 k_y y \qquad (16)$$

which is the form suggested in the analytic nonlinear mode coupling work of CHATURVEDI and OSSAKOW (1977). In addition, the following values were taken: $k_y = k_x = 2\pi/960m$, $A_{1,1} = 10^{-4}$, and $A_{2,0} = 2 \times 10^{-6}$.

The nonlinear aspects of these simulations for the L = 10 km case are shown in figs. 7-9. Figure 7a shows an isodensity contour plot of $\tilde{n}/n_o$ at t = 0. The contours describe a sequence of enhancements and depletions arranged in a checkerboard fashion in line with the initial perturbation given by (16). Figures 7b and 7c show the time evolution of the initial perturbation at t = 3000 and 6000 sec., respectively. The density fluctuation contours at t = 10,000 sec. are depicted in fig. 7d and here some vertical elongation and steepening can be observed along with small scale structures. In figs. 8a and 8b representative one dimensional horizontal $P(k_x)$ and

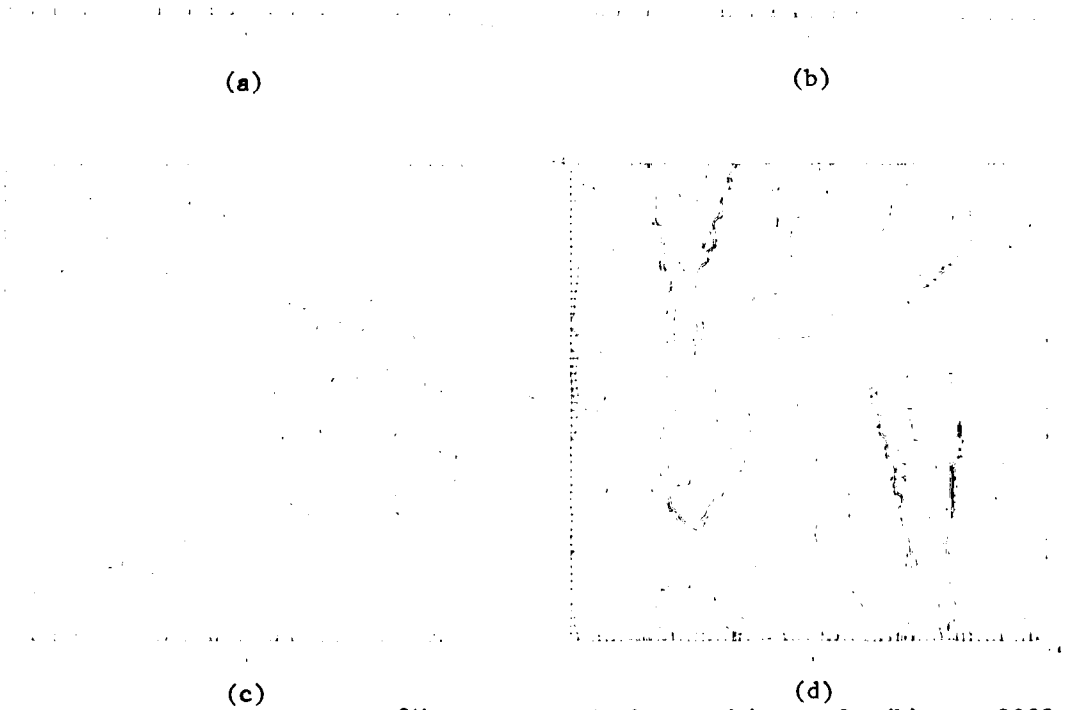

Fig. 7 - Isodensity contours of $\tilde{n}/n_o$ for L = 10 km at (a) t = 0, (b) t = 3000 s., (c) 6000 s., and (d) t = 10,000 s. Solid contours denote $\tilde{n}/n_o > 0$; dashed contours denote $n/n_o < 0$. All contours are evenly spaced with the y axis vertical and the x axis horizontal. The tick marks represent grid point location (after KESKINEN et al., 1980).

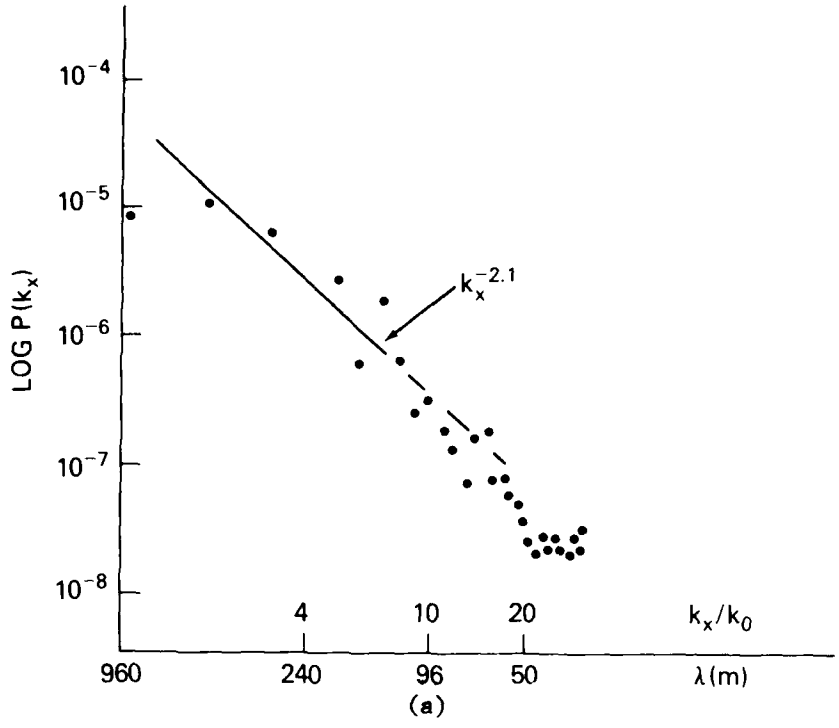

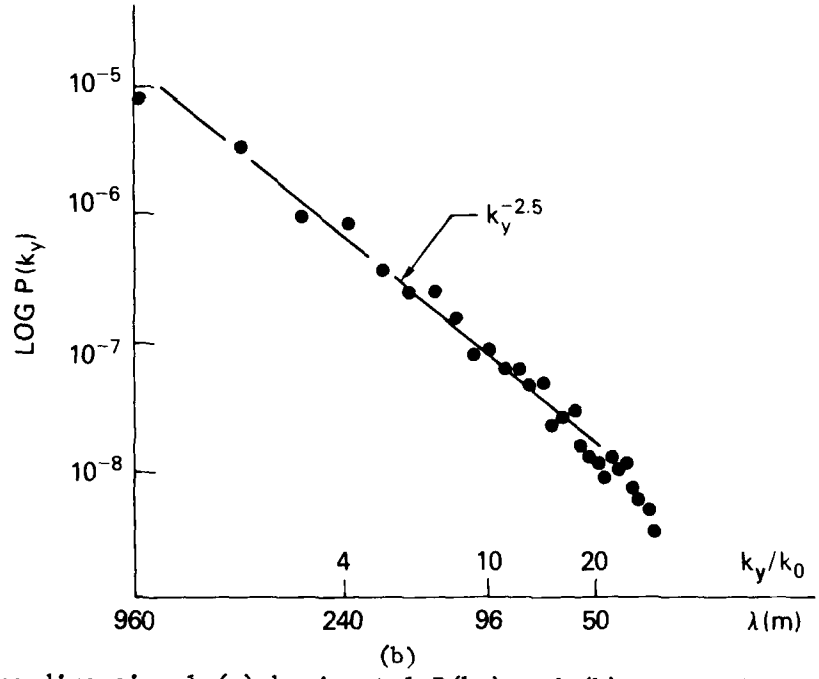

Fig. 8 - One dimensional (a) horizontal $P(k_x)$ and (b) vertical $P(k_y)$ power spectra versus k_x and k_y, respectively, for L ≈ 10 km at t = 10,000 s. The solid curves are the least squares fit to the results from the numerical simulations (dots), and $k_o = 2\pi/960$m is the fundamental wave number.

vertical $P(k_y)$ power spectra, in the nonlinear late time regime (t = 10,000 sec.), have been plotted. In this saturated regime we see that $P(k_x) \propto k_x^{-2.1}$ and $P(k_y) \propto k_y^{-2.5}$, for $\lambda \sim 70$ - 960m. These spectral indices are in agreement with experimental observations (DYSON et al., 1974; COSTA and KELLEY, 1978a), global numerical simulations (SCANNAPIECO and OSSAKOW, 1976) and nonlinear analytic theory (CHATURVEDI and OSSAKOW, 1977). Figure 9 depicts the evolution of the $A_{1,1}$ and $A_{2,0}$ modes. Initially, the $A_{2,0}$ vertical mode is damped as predicted by linear theory. As the linearly unstable $A_{1,1}$ mode increases it nonlinearly triggers the growth of $A_{2,0}$. At late times, these two modes arrange themselves in accord with the nonlinear theoretical predictions of CHATURVEDI and OSSAKOW (1977). From fig. 9, we note that in the quasi-final state $A_{2,0} < A_{1,1}$; whereas, for the L = 5 km case depicted in KESKINEN et al. (1980) $A_{2,0} > A_{1,1}$ (the corresponding figures in KESKINEN et al., 1980, to those shown here as figs. 8 and 9, are for L = 15 and L = 5 km, respectively and so are not the L = 10 km case).

CHATURVEDI and OSSAKOW (1977) showed that for a two dimensional perturbation of the form (16), the dominant nonlinearity in the continuity equation is the $\underline{V}_{\underline{EXB}} \cdot \nabla n$ term. Taking $\tilde{n}/n_o = A_{1,1} \sin(k_x x - \omega t)\cos k_y y + A_{2,0} \sin 2k_y y$ gives the equation for $A_{1,1}$ and $A_{2,0}$

$$\frac{\partial A_{1,1}}{\partial t} = \gamma_{1,1} A_{1,1} - 2 \alpha A_{1,1} A_{2,0} \tag{17}$$

$$\frac{\partial A_{2,0}}{\partial t} = - |\gamma_{2,0}| A_{2,0} + \frac{\alpha}{2} A_{1,1}^2 \tag{18}$$

where

$$\gamma_{1,1} = \frac{g}{2\nu_{in}} \frac{}{L} - \nu_R \quad , \quad L^{-1} = \frac{1}{n_o} \frac{\partial n_o}{\partial y} \tag{19}$$

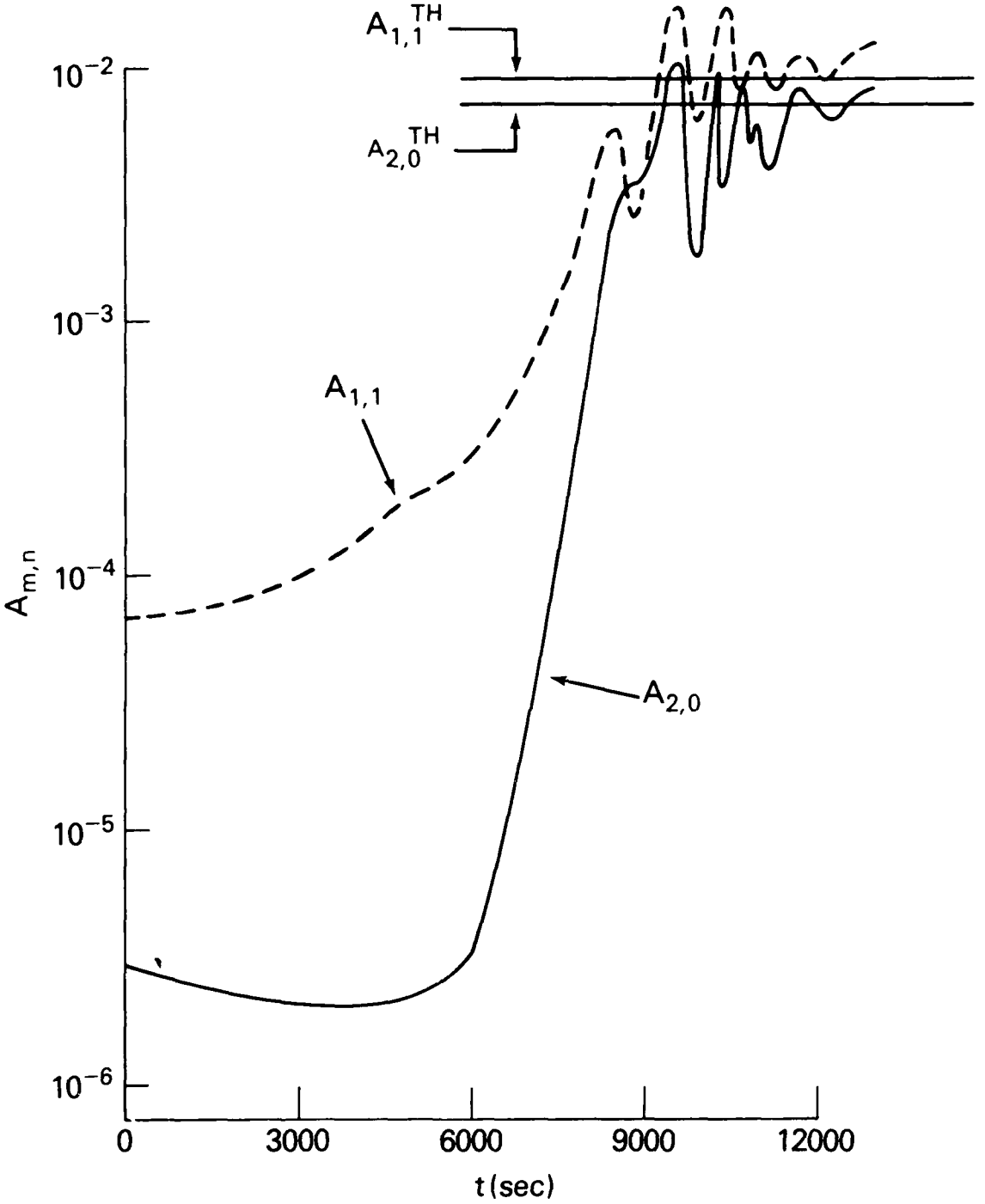

Fig. 9 - Time history of mode amplitudes $A_{2,0}$ (vertical mode) and $A_{1,1}$ for L = 10 km, where $A_{m,n} = A_{mk_{oy},nk_{ox}}$ and $k_{oy} = k_{ox} = 2\pi/960$m. The horizontal solid lines are the steady state amplitudes of $A_{1,1}^{TH}$ and $A_{2,0}^{TH}$ from the theory of CHATURVEDI and OSSAKOW (1977).

$$\gamma_{2,0} = -\nu_R \tag{20}$$

$$\alpha = \frac{k_y k_x^2 g}{k^2 \nu_{in}}, \quad k^2 = k_x^2 + k_y^2 \tag{21}$$

At saturation $\partial A_{1,1}/\partial t = \partial A_{2,0}/\partial t = 0$ and we obtain

$$A_{2,0} = \frac{\gamma_{1,1}}{2\alpha} \approx \frac{1}{2k_y L} \tag{22}$$

$$A_{1,1} = \left(\frac{2|\gamma_{2,0}|}{\alpha} A_{2,0}\right)^{1/2} \approx \left(\frac{k^2}{k_x^2} \frac{\nu_R \nu_{in}}{gL\, k_y^2}\right)^{1/2} \tag{23}$$

It is (22) and (23) which are given as $A^{TH}_{2,0}$ and $A^{TH}_{1,1}$ in fig. 9 (with ν_{in} = 0.6 s^{-1}, $\nu_R = 3 \times 10^{-4}$ s^{-1}).

The results gleaned from these intermediate wavelength collisional R-T instability numerical simulations in the nighttime equatorial F region are: (i) linearly unstable modes saturate by nonlinear excitation of linearly damped vertical modes; (ii) a vertical elongation is observed along with small scale structure; and (iii) the one dimensional vertical and horizontal power spectra for the plasma density fluctuations $\propto k^{-n}$, where n = 2-2.5.

ESF Simulation Results in General

We can summarize the nonlinear numerical simulation results, to date, as follows. The collisional R-T instability can cause linear growth on the bottomside of the ESF region. Plasma depletions (bubbles) form on the bottomside, steepen on their top and nonlinearly rise to the topside above the F peak by polarization E X B motion. High altitude of the F peak, small bottomside background electron density gradient scale lengths, and large percentage depletions yield large vertical bubble rise velocities, with the first two conditions favoring collisional R-T growth. Horizontally large

spatial bubbles ($\sim$ 50 - 100 km widths) can be produced by long wavelength perturbations. Preliminary results (CHATURVEDI et al., 1978) show that westward drifts of the bubbles, with respect to the main plasma, can be produced by an eastward neutral wind. Results of intermediate wavelength (100m - 1 km) simulations, of the collisional R-T instability in local regions, show saturation by nonlinear generation of linearly damped vertical modes and a one dimensional power spectrum $\propto k^{-n}$, where n = 2-2.5.

Very Small Scale ($\leq$ 10m) Irregularities

We will not dwell much in this area because another paper in this edition can be found on the subject. Some basic ideas will be presented. The work in this section is being applied to account for the coherent backscatter radar measurements made of small scale irregularities at various equatorial locations (3m at Jicamarca, Peru; 1m, 36 cm, and 11 cm at Kwajalein, Marshall Islands). The calculations are multilinear, using kinetic theory and result in various plasma kinetic drift wave modes. Kinetic theory is used because of the small sizes involved (remembering that the ion gyroradius is $\sim$ 6m for the ESF ionosphere). It is multilinear because it depends on a two-step process whereby linear theory is performed on the nonlinear state. By using linear theory we are attempting to account for the radar observed irregularities by the simplest means, i.e., linear excitation. This does not preclude their being excited by truly nonlinear means. However, if they can be excited in a linear fashion this will give us a warm feeling. The driving density gradients, in these calculations, are thought to arise through a primary instability (e.g., long wavelength collisional R-T instability), driven by the zero order background ionospheric equatorial F region vertical electron density gradient, achieving a large amplitude state. The zero order ionospheric electron density gradient is of larger

scale size than the primary instability electron density gradient scale size, which would be of the order of the instability wavelength. Because the calculations are kinetic they employ particle distribution functions, which would be described by a Vlasov equation in the collisionless limit (COSTA and KELLEY, 1978b) and contain an additional collision operator, i.e., a Fokker-Planck type equation, in the collisional regime (see HUBA and OSSAKOW, 1979a;b; 1980; SPERLING and GOLDMAN, 1980).

We will present some general concepts regarding kinetic drift waves which will be useful for the calculations which have been done. The basic geometry is such that

$$\underline{B} = B\,\hat{z} \tag{24}$$

$$n_o = n_o(x) \tag{25}$$

(similar to the zero order background equatorial ionospheric geometry) where here $n_o(x)$ arises due to the primary instability. The orthogonal coordinate system is completed by the ion and electron diamagnetic velocities being along the y axis,

$$\underline{V}_d = (V_{di} - V_{de})\,\hat{y} \tag{26}$$

$$V_{di} = (V_i^2/2\Omega_i)\,(\partial \ln n_o/\partial x) \tag{27}$$

$$V_{de} = -\,(V_e^2/2\Omega_e)\,(\partial \ln n_o/\partial x) \tag{28}$$

where $V_{i,e} = (2T_{i,e}/m_{i,e})^{1/2}$ and the larmor radius is defined by $r_\alpha = V_\alpha/\Omega_\alpha$. The linear analysis is then performed with this in mind.

First the low frequency, $\omega \ll \Omega_i$, collisionless drift wave calculations of COSTA and KELLEY (1978a;b) for $k\,r_i \sim 1$ were performed to explain the 3m

ESF irregularities observed by the Jicamarca radar (50 MHz) in the coherent backscatter mode. HUBA and OSSAKOW (1979a) included electron-ion, electron-neutral, and ion-ion collisions in the low frequency drift waves and showed that linear theory could not explain the 3m regime. The theory could only show instability down to ~ 10m for reasonable ESF plasma densities and density gradient scale lengths.

In a series of papers, the linear theory of high frequency, $\omega \gtrsim \Omega_i$, drift waves (HUBA et al., 1978; HUBA and OSSAKOW, 1979b; 1980; SPERLING and GOLDMAN, 1980) for $kr_i \gtrsim 1$ and $kr_e \sim 1$ have been investigated including, at various stages, ion-ion, electron-electron, electron-ion, and electron-neutral collisional effects. These studies have been undertaken to account for the 1m, 36 cm, and 11 cm ESF irregularities observed at Kwajalein with the ALTAIR (155 MHz and 415 MHz) and TRADEX (1320 MHz) radars operating in the coherent backscatter modes. These wavelengths appear to be explainable by the linear theory of the high frequency lower hybrid drift instability favoring low densities and steep plasma density gradients. Consequently, within the context of linear theory while these high frequency instabilities can go up to ~ 1m and the low frequency instabilities can go down to ~ 10m, there is a gray area between 1-10m that is inaccessible by linear theory.

CONCLUSIONS AND SUMMARY

The basic physical picture of ESF that emerges is as follows. After sunset the E region begins to recombine and there is effectively no E region conductivity to short out any irregularities in the F region. Due to recombination and possible electrodynamic effects (upward motion of the F region plasma due to $\underline{E} \times \underline{B}$) the bottomside F region background electron density gradient begins to steepen. The steepening due to plasma $\underline{E} \times \underline{B}$ uplift

caused by an eastward electric field is much like barium cloud steepening in equatorial geometry (note a downward motion of the neutral atmosphere will have the same effect). When the altitude of the F region is high enough and/or the bottomside background electron density gradient steep enough to overcome recombination effects, plasma density fluctuations will begin to grow on the bottomside via the collisional Rayleigh-Taylor instability mechanism (or possibly initiated by the $\underline{E} \times \underline{B}$ gradient drift instability; in any case a fluid type gradient instability). These irregularities will in turn form plasma density depletions (bubbles) on the bottomside which will then nonlinearly rise by polarization $\underline{E} \times \underline{B}$ motion through the F peak and cause topside spread F. (The higher the F peak and/or the sharper the bottomside gradient, and the higher the % depletion the faster the rise rate of the bubble and the faster the evolution of ESF.) These steepening bubbles (on their topside) can then bifurcate and form smaller scale structure by a cascade or two-step mechanism. An eastward neutral wind can cause the bubbles to move westward with respect to the bulk plasma motion. The long wavelength irregularities have a power law PSD $\propto k^{-2\pm?}$. It is presently believed that the small scale ($\lesssim$ 3m) radar backscatter observed irregularities (kinetic type instabilities) are created by the steep plasma density gradients created by the primary long wavelength fluid type instabilities (collisional Rayleigh-Taylor, etc.). The turn on and turn off of these very small scale irregularities and their connection to the longer wavelength irregularities is not well understood at present and requires further investigation.

Although much work has been done in recent years on ESF and a coherent picture is emerging, there are still remaining problems worthy of investigation. Some of these problems are as follows. (1) The relation of the very small scale radar observed irregularities to the longer wavelength

irregularities is not well understood. (a) Quantitatively, what are the turn on and turn off criteria for these very small scale lengths? (b) A more complete study of the collisional effects on plasma kinetic drift wave instabilities is required. (c) A determination of the nonlinear saturation of the small scale irregularities, including saturated amplitudes and power spectra, is needed. (2) The effects of ion inertia, including the investigation of topside structure, plasma bubble evolution into collisionless altitudes ($\nu_{in}^2 \ll 4g/L$), nonlinear saturation, and bubble pinch off or wedge formation has to be studied. (3) We need to do an investigation of the effects of neutral winds, electric fields, and changing initial conditions on our previous plasma fluid long wavelength studies (particularly the numerical simulations). (4) An analytic description of many ESF bubbles is lacking. Also, how do they decay and what is the role of diffusion? (5) There is a need to study three dimensional effects, including the effects of $k_{\parallel}$ (wavenumber parallel to $\underline{B}$). (6) The effects of other regions of the ionosphere, e.g., the E region, needs to be investigated. These problem areas should keep us busy for the foreseeable future.

ACKNOWLEDGMENTS

This work was supported by the Defense Nuclear Agency and the Office of Naval Research. The author is grateful to his colleagues and their endeavors to provide an understanding of ESF phenomena. In particular, I am deeply indebted to Pradeep Chaturvedi, Joe Huba, Mike Keskinen (also for providing figs. 8 and 9), Ed McDonald, Tony Scannapieco and Steve Zalesak without whose support this article could not have been written.

REFERENCES

ANDERSON, D. N. and HAERENDEL, G.	1979	J. Geophys. Res. 84, 4251
BALSLEY, B. B., HAERENDEL, G. and GREENWALD, R. A.	1972	J. Geophys. Res. 77, 5625
BOOKER, H. G. and WELLS, H. W.	1938	Terres. Magn. 43, 249
BURKE, W. J.	1979	Planet. Space Sci. 27, 1187
CALVERT, W.	1963	J. Geophys. Res. 68, 2591
CHATURVEDI, P. K. and KAW, P. K.	1975a	Geophys. Res. Lett. 2, 381
CHATURVEDI, P. K. and KAW, P. K.	1975b	Geophys. Res. Lett. 2, 499
CHATURVEDI, P. and KAW, P.	1976	J. Geophys. Res. 81, 3257
CHATURVEDI, P. K. and OSSAKOW, S. L.	1977	Geophys. Res. Lett. 4, 558
CHATURVEDI, P. K., ZALESAK, S. T. and OSSAKOW, S. L.	1978	Eos Trans. Am. Geophys. Un. 59, 1144
CHIU, Y. T. and STRAUS, J. M.	1979	J. Geophys. Res. 84, 3283
COSTA, E. and KELLEY, M. C.	1978a	J. Geophys. Res. 83, 4359
COSTA, E. and KELLEY, M. C.	1978b	J. Geophys. Res. 83, 4365
DAGG, M.	1957	J. Atmos. Terr. Phys. 11, 139
DUNGEY, J. W.	1956	J. Atmos. Terr. Phys. 9, 304
DYSON, P. L., McCLURE, J. P. and HANSON, W. B.	1974	J. Geophys. Res. 79, 1497
FARLEY, D. T., BALSLEY, B. B., WOODMAN, R. F. and McCLURE, J. P.	1970	J. Geophys. Res. 75, 7199
HAERENDEL, G.	1972	Eos Trans. Am. Geophys. Un. 53, 1082
HAERENDEL, G.	1974	Preprint, Max-Planck Institute fur Physik und Astrophysik, Garching, West Germany

HUBA, J. D. and OSSAKOW, S. L.	1979a	J. Geophys. Res. 84, 6697
HUBA, J. D. and OSSAKOW, S. L.	1979b	Phys. Fluids 22, 1349
HUBA, J. D. and OSSAKOW, S. L.	1980	J. Geophys. Res. (in press)
HUBA, J. D., CHATURVEDI, P. K., OSSAKOW, S. L. and TOWLE, D. M.	1978	Geophys. Res. Lett. 5, 695
HUDSON, M. K.	1978	J. Geophys. Res. 83, 3189
HUDSON, M. K. and KENNEL, C. F.	1975	J. Geophys. Res. 60, 4581
HUDSON, M. K., KENNEL, C. F. and KAW, P. K.	1973	Eos Trans. Am. Geophys. Un. 54, 1147
KELLEY, M. C., HAERENDEL, L. G. KAPPLER, H., VALENZUELA, A., BALSLEY, B. B., CARTER, D. A., ECKLUND, W. L., CARLSON, C. W., HAUSLER, B. and TORBERT, R.	1976	Geophys. Res. Lett. 3, 448
KELLEY, M. C. and OTT, E.	1978	J. Geophys. Res. 83, 4369
KESKINEN, M. J., OSSAKOW, S. L. and CHATURVEDI, P. K.	1980	J. Geophys. Res. 85, 1775
MARTYN, D. F.	1959	J. Geophys. Res. 64, 2178
McCLURE, J. P., HANSON, W. B. and HOFFMAN, J. H.	1977	J. Geophys. Res. 82, 2650
OSSAKOW, S. L. and CHATURVEDI, P. K.	1978	J. Geophys. Res. 83, 2085
OSSAKOW, S. L., ZALESAK, S. T., McDONALD, B. E. and CHATURVEDI, P. K.	1979	J. Geophys. Res. 84, 17
OTT, E.	1978	J. Geophys. Res. 83, 2066
SCANNAPIECO, A. J. and OSSAKOW, S. L.	1976	Geophys. Res. Lett. 3, 451

SPERLING, J. L. and GOLDMAN, S. R. 1980 J. Geophys. Res. 85, 3494

SZUSZCZEWICZ, E. P. 1978 J. Geophys. Res. 83, 2665

WOODMAN, R. F. and LA HOZ, C. 1976 J. Geophys. Res. 81, 5447

ZALESAK, S. T. and OSSAKOW, S. L. 1980 J. Geophys. Res. 85, 2131

DISTRIBUTION LIST

DEPARTMENT OF DEFENSE

ASSISTANT SECRETARY OF DEFENSE
COMM, CMD, CONT & INTELL
WASHINGTON, D.C. 20301
01CY ATTN J. BABCOCK
01CY ATTN M. EPSTEIN

ASSISTANT TO THE SECRETARY OF DEFENSE
ATOMIC ENERGY
WASHINGTON, D.C. 20301
01CY ATTN EXECUTIVE ASSISTANT

DIRECTOR
COMMAND CONTROL TECHNICAL CENTER
PENTAGON RM BE 685
WASHINGTON, D.C. 20301
01CY ATTN C-650
01CY ATTN C-312 R. MASON

DIRECTOR
DEFENSE ADVANCED RSCH PROJ AGENCY
ARCHITECT BUILDING
1400 WILSON BLVD.
ARLINGTON, VA. 22209
01CY ATTN NUCLEAR MONITORING RESEARCH
01CY ATTN STRATEGIC TECH OFFICE

DEFENSE COMMUNICATION ENGINEER CENTER
1860 WIEHLE AVENUE
RESTON, VA. 22090
01CY ATTN CODE R820
01CY ATTN CODE R410 JAMES W. MCLEAN
01CY ATTN CODE R720 J. WORTHINGTON

DIRECTOR
DEFENSE COMMUNICATIONS AGENCY
WASHINGTON, D.C. 20305
(ADR CNWDI: ATTN CODE 240 FOR)
01CY ATTN CODE 101B

DEFENSE TECHNICAL INFORMATION CENTER
CAMERON STATION
ALEXANDRIA, VA. 22314
(12 COPIES IF OPEN PUBLICATION, OTHERWISE 2 COPIES)
12CY ATTN TC

DIRECTOR
DEFENSE INTELLIGENCE AGENCY
WASHINGTON, D.C. 20301
01CY ATTN DT-1B
01CY ATTN DB-4C E. O'FARRELL
01CY ATTN DIAAP A. WISE
01CY ATTN DIAST-5
01CY ATTN DT-1BZ R. MORTON
01CY ATTN HQ-TR J. STEWART
01CY ATTN W. WITTIG DC-7D

DIRECTOR
DEFENSE NUCLEAR AGENCY
WASHINGTON, D.C. 20305
01CY ATTN STVL
04CY ATTN TITL
01CY ATTN DDST
03CY ATTN RAAE

COMMANDER
FIELD COMMAND
DEFENSE NUCLEAR AGENCY
KIRTLAND AFB, NM 87115
01CY ATTN FCPR

DIRECTOR
INTERSERVICE NUCLEAR WEAPONS SCHOOL
KIRTLAND AFB, NM 87115
01CY ATTN DOCUMENT CONTROL

JOINT CHIEFS OF STAFF
WASHINGTON, D.C. 20301
01CY ATTN J-3 WWMCCS EVALUATION OFFICE

DIRECTOR
JOINT STRAT TGT PLANNING STAFF
OFFUTT AFB
OMAHA, NB 68113
01CY ATTN JLTW-2
01CY ATTN JPST G. GOETZ

CHIEF
LIVERMORE DIVISION FLD COMMAND DNA
DEPARTMENT OF DEFENSE
LAWRENCE LIVERMORE LABORATORY
P. O. BOX 808
LIVERMORE, CA 94550
01CY ATTN FCPRL

DIRECTOR
NATIONAL SECURITY AGENCY
DEPARTMENT OF DEFENSE
FT. GEORGE G. MEADE, MD 20755
01CY ATTN JOHN SKILLMAN R52
01CY ATTN FRANK LEONARD
01CY ATTN W14 PAT CLARK
01CY ATTN OLIVER H. BARTLETT W32
01CY ATTN R5

COMMANDANT
NATO SCHOOL (SHAPE)
APO NEW YORK 09172
01CY ATTN U.S. DOCUMENTS OFFICER

UNDER SECY OF DEF FOR RSCH & ENGRG
DEPARTMENT OF DEFENSE
WASHINGTON, D.C. 20301
01CY ATTN STRATEGIC & SPACE SYSTEMS (OS)

WWMCCS SYSTEM ENGINEERING ORG
WASHINGTON, D.C. 20305
01CY ATTN R. CRAWFORD

COMMANDER/DIRECTOR
ATMOSPHERIC SCIENCES LABORATORY
U.S. ARMY ELECTRONICS COMMAND
WHITE SANDS MISSILE RANGE, NM 88002
01CY ATTN DELAS-EO F. NILES

DIRECTOR
BMD ADVANCED TECH CTR
HUNTSVILLE OFFICE
P. O. BOX 1500
HUNTSVILLE, AL 35807
01CY ATTN ATC-T MELVIN T. CAPPS
01CY ATTN ATC-O W. DAVIES
01CY ATTN ATC-R DON RUSS

PROGRAM MANAGER
BMD PROGRAM OFFICE
5001 EISENHOWER AVENUE
ALEXANDRIA, VA 22333
01CY ATTN DACS-BMT J. SHEA

CHIEF C-E SERVICES DIVISION
U.S. ARMY COMMUNICATIONS CMD
PENTAGON RM 1B269
WASHINGTON, D.C. 20310
01CY ATTN C-E-SERVICES DIVISION

COMMANDER
FRADCOM TECHNICAL SUPPORT ACTIVITY
DEPARTMENT OF THE ARMY
FORT MONMOUTH, N.J. 07703
01CY ATTN DRSEL-NL-RD H. BENNET
01CY ATTN DRSEL-PL-ENV H. BOMKE
01CY ATTN J. E. QUIGLEY

COMMANDER
HARRY DIAMOND LABORATORIES
DEPARTMENT OF THE ARMY
2800 POWDER MILL ROAD
ADELPHI, MD 20783
(CNWDI-INNER ENVELOPE: ATTN: DELHD-RBH)
01CY ATTN DELHD-TI M. WEINER
01CY ATTN DELHD-RB R. WILLIAMS
01CY ATTN DELHD-NP F. WIMENITZ
01CY ATTN DELHD-NP C. MOAZED

COMMANDER
U.S. ARMY COMM-ELEC ENGRG INSTAL AGY
FT. HUACHUCA, AZ 85613
01CY ATTN CCC-EMEO GEORGE LANE

COMMANDER
U.S. ARMY FOREIGN SCIENCE & TECH CTR
220 7TH STREET, NE
CHARLOTTESVILLE, VA 22901
01CY ATTN DRXST-SD
01CY ATTN R. JONES

COMMANDER
U.S. ARMY MATERIEL DEV & READINESS CMD
5001 EISENHOWER AVENUE
ALEXANDRIA, VA 22333
01CY ATTN DRCLDC J. A. BENDER

COMMANDER
U.S. ARMY NUCLEAR AND CHEMICAL AGENCY
7500 BACKLICK ROAD
BLDG 2073
SPRINGFIELD, VA 22150
01CY ATTN LIBRARY

DIRECTOR
U.S. ARMY BALLISTIC RESEARCH LABS
ABERDEEN PROVING GROUND, MD 21005
01CY ATTN TECH LIB EDWARD BAICY

COMMANDER
U.S. ARMY SATCOM AGENCY
FT. MONMOUTH, NJ 07703
01CY ATTN DOCUMENT CONTROL

COMMANDER
U.S. ARMY MISSILE INTELLIGENCE AGENCY
REDSTONE ARSENAL, AL 35809
01CY ATTN JIM GAMBLE

DIRECTOR
U.S. ARMY TRADOC SYSTEMS ANALYSIS ACTIVITY
WHITE SANDS MISSILE RANGE, NM 88002
01CY ATTN ATAA-SA
01CY ATTN TCC/F. PAYAN JR.
01CY ATTN ATAA-TAC LTC J. HESSE

COMMANDER
NAVAL ELECTRONIC SYSTEMS COMMAND
WASHINGTON, D.C. 20360
01CY ATTN NAVALEX 034 T. HUGHES
01CY ATTN PME 117
01CY ATTN PME 117-T
01CY ATTN CODE 5011

COMMANDING OFFICER
NAVAL INTELLIGENCE SUPPORT CTR
4301 SUITLAND ROAD, BLDG. 5
WASHINGTON, D.C. 20390
01CY ATTN MR. DUBBIN STIC 12
01CY ATTN NISC-50
01CY ATTN CODE 5404 J. GALET

COMMANDER
NAVAL OCEAN SYSTEMS CENTER
SAN DIEGO, CA 92152
03CY ATTN CODE 532 W. MOLER
01CY ATTN CODE 0230 C. BAGGETT
01CY ATTN CODE 81 R. EASTMAN

DIRECTOR
NAVAL RESEARCH LABORATORY
WASHINGTON, D.C. 20375
01CY ATTN CODE 4700 T. P. COFFEY (25 CYS IF UN, 1 CY IF CLASS)
01CY ATTN CODE 4701 JACK D. BROWN
01CY ATTN CODE 4780 BRANCH HEAD (150 CYS IF UN, 1 CY IF CLASS)
01CY ATTN CODE 7500 HQ COMM DIR BRUCE WALD
01CY ATTN CODE 7550 J. DAVIS
01CY ATTN CODE 7580
01CY ATTN CODE 7551
01CY ATTN CODE 7555
01CY ATTN CODE 4730 E. MCLEAN
01CY ATTN CODE 4127 C. JOHNSON

COMMANDER
NAVAL SEA SYSTEMS COMMAND
WASHINGTON, D.C. 20362
01CY ATTN CAPT R. PITKIN

COMMANDER
NAVAL SPACE SURVEILLANCE SYSTEM
DAHLGREN, VA 22448
01CY ATTN CAPT J. H. BURTON

OFFICER-IN-CHARGE
NAVAL SURFACE WEAPONS CENTER
WHITE OAK, SILVER SPRING, MD 20910
01CY ATTN CODE F31

DIRECTOR
STRATEGIC SYSTEMS PROJECT OFFICE
DEPARTMENT OF THE NAVY
WASHINGTON, D.C. 20376
01CY ATTN NSP-2141
01CY ATTN NSSP-2722 FRED WIMBERLY

NAVAL SPACE SYSTEM ACTIVITY
P. O. BOX 92960
WORLDWAY POSTAL CENTER
LOS ANGELES, CALIF. 90009
01CY ATTN A. B. HAZZARD

COMMANDER
NAVAL SURFACE WEAPONS CENTER
DAHLGREN LABORATORY
DAHLGREN, VA 22448
01CY ATTN CODE DF-14 R. BUTLER

COMMANDING OFFICER
NAVY SPACE SYSTEMS ACTIVITY
P.O. BOX 92960
WORLDWAY POSTAL CENTER
LOS ANGELES, CA. 90009
01CY ATTN CODE 52

OFFICE OF NAVAL RESEARCH
ARLINGTON, VA 22217
01CY ATTN CODE 465
01CY ATTN CODE 461
01CY ATTN CODE 402
01CY ATTN CODE 420
01CY ATTN CODE 421

COMMANDER
AEROSPACE DEFENSE COMMAND/DC
DEPARTMENT OF THE AIR FORCE
ENT AFB, CO 80912
01CY ATTN DC MR. LONG

COMMANDER
AEROSPACE DEFENSE COMMAND/XPD
DEPARTMENT OF THE AIR FORCE
ENT AFB, CO 80912
01CY ATTN XPDQQ
01CY ATTN XP

AIR FORCE GEOPHYSICS LABORATORY
HANSCOM AFB, MA 01731
01CY ATTN OPR HAROLD GARDNER
01CY ATTN OPR-1 JAMES C. ULWICK
01CY ATTN LKB KENNETH S. W. CHAMPION
01CY ATTN OPR ALVA T. STAIR
01CY ATTN PHP JULES AARONS
01CY ATTN PHD JURGEN BUCHAU
01CY ATTN PHD JOHN P. MULLEN

AF WEAPONS LABORATORY
KIRTLAND AFB, NM 87117
01CY ATTN SUL
01CY ATTN CA ARTHUR H. GUENTHER
01CY ATTN DYC CAPT J. BARRY
01CY ATTN DYC JOHN M. KAMM
01CY ATTN DYT CAPT MARK A. FRY
01CY ATTN DES MAJ GARY GANONG
01CY ATTN DYC J. JANNI

AFTAC
PATRICK AFB, FL 32925
01CY ATTN TF/MAJ WILEY
01CY ATTN TN

AIR FORCE AVIONICS LABORATORY
WRIGHT-PATTERSON AFB, OH 45433
01CY ATTN AAD WADE HUNT
01CY ATTN AAD ALLEN JOHNSON

DEPUTY CHIEF OF STAFF
RESEARCH, DEVELOPMENT, & ACQ
DEPARTMENT OF THE AIR FORCE
WASHINGTON, D.C. 20330
01CY ATTN AFRDQ

HEADQUARTERS
ELECTRONIC SYSTEMS DIVISION/XR
DEPARTMENT OF THE AIR FORCE
HANSCOM AFB, MA 01731
01CY ATTN XR J. DEAS

HEADQUARTERS
ELECTRONIC SYSTEMS DIVISION/YSEA
DEPARTMENT OF THE AIR FORCE
HANSCOM AFB, MA 01731
01CY ATTN YSEA

HEADQUARTERS
ELECTRONIC SYSTEMS DIVISION/DC
DEPARTMENT OF THE AIR FORCE
HANSCOM AFB, MA 01731
01CY ATTN DCKC MAJ J.C. CLARK

COMMANDER
FOREIGN TECHNOLOGY DIVISION, AFSC
WRIGHT-PATTERSON AFB, OH 45433
01CY ATTN NICD LIBRARY
01CY ATTN ETDP B. BALLARD

COMMANDER
ROME AIR DEVELOPMENT CENTER, AFSC
GRIFFISS AFB, NY 13441
01CY ATTN DOC LIBRARY/TSLD
01CY ATTN OCSE V. COYNE

SAMSO/SZ
POST OFFICE BOX 92960
WORLDWAY POSTAL CENTER
LOS ANGELES, CA 90009
(SPACE DEFENSE SYSTEMS)
01CY ATTN SZJ

STRATEGIC AIR COMMAND/XPFS
OFFUTT AFB, NB 68113
01CY ATTN XPFS MAJ B. STEPHAN
01CY ATTN ADWATE MAJ BRUCE BAUER
01CY ATTN NRT
01CY ATTN DOK CHIEF SCIENTIST

SAMSO/SK
P. O. BOX 92960
WORLDWAY POSTAL CENTER
LOS ANGELES, CA 90009
01CY ATTN SKA (SPACE COMM SYSTEMS) M. CLAVIN

SAMSO/MN
NORTON AFB, CA 92409
(MINUTEMAN)
01CY ATTN MNNL LTC KENNEDY

COMMANDER
ROME AIR DEVELOPMENT CENTER, AFSC
HANSCOM AFB, MA 01731
01CY ATTN EEP A. LORENTZEN

DEPARTMENT OF ENERGY
ALBUQUERQUE OPERATIONS OFFICE
P. O. BOX 5400
ALBUQUERQUE, NM 87115
01CY ATTN DOC CON FOR D. SHERWOOD

DEPARTMENT OF ENERGY
LIBRARY ROOM G-042
WASHINGTON, D.C. 20545
01CY ATTN DOC CON FOR A. LABOWITZ

EG&G, INC.
LOS ALAMOS DIVISION
P. O. BOX 809
LOS ALAMOS, NM 85544
01CY ATTN DOC CON FOR J. BREEDLOVE

UNIVERSITY OF CALIFORNIA
LAWRENCE LIVERMORE LABORATORY
P. O. BOX 808
LIVERMORE, CA 94550
01CY ATTN DOC CON FOR TECH INFO DEPT
01CY ATTN DOC CON FOR L-389 R. OTT
01CY ATTN DOC CON FOR L-31 R. MAGER
01CY ATTN DOC CON FOR L-46 F. SEWARD

LOS ALAMOS SCIENTIFIC LABORATORY
P. O. BOX 1663
LOS ALAMOS, NM 87545
01CY ATTN DOC CON FOR J. WOLCOTT
01CY ATTN DOC CON FOR R. F. TASCHEK
01CY ATTN DOC CON FOR E. JONES
01CY ATTN DOC CON FOR J. MALIK
01CY ATTN DOC CON FOR R. JEFFRIES
01CY ATTN DOC CON FOR J. ZINN
01CY ATTN DOC CON FOR P. KEATON
01CY ATTN DOC CON FOR D. WESTERVELT

SANDIA LABORATORIES
P. O. BOX 5800
ALBUQUERQUE, NM 87115
01CY ATTN DOC CON FOR J. MARTIN
01CY ATTN DOC CON FOR W. BROWN
01CY ATTN DOC CON FOR A. THORNBROUGH
01CY ATTN DOC CON FOR T. WRIGHT
01CY ATTN DOC CON FOR D. DAHLGREN
01CY ATTN DOC CON FOR 3141
01CY ATTN DOC CON FOR SPACE PROJECT DIV

SANDIA LABORATORIES
LIVERMORE LABORATORY
P. O. BOX 969
LIVERMORE, CA 94550
01CY ATTN DOC CON FOR B. MURPHEY
01CY ATTN DOC CON FOR T. COOK

OFFICE OF MILITARY APPLICATION
DEPARTMENT OF ENERGY
WASHINGTON, D.C. 20545
01CY ATTN DOC CON FOR D. GALE

OTHER GOVERNMENT

CENTRAL INTELLIGENCE AGENCY
ATTN RD/SI, RM 5G48, HQ BLDG
WASHINGTON, D.C. 20505
01CY ATTN OSI/PSID RM 5F 19

DEPARTMENT OF COMMERCE
NATIONAL BUREAU OF STANDARDS
WASHINGTON, D.C. 20234
(ALL CORRES: ATTN SEC OFFICER FOR)
01CY ATTN R. MOORE

INSTITUTE FOR TELECOM SCIENCES
NATIONAL TELECOMMUNICATIONS & INFO ADMIN
BOULDER, CO 80303
01CY ATTN A. JEAN (UNCLASS ONLY)
01CY ATTN W. UTLAUT
01CY ATTN D. CROMBIE
01CY ATTN L. BERRY

NATIONAL OCEANIC & ATMOSPHERIC ADMIN
ENVIRONMENTAL RESEARCH LABORATORIES
DEPARTMENT OF COMMERCE
BOULDER, CO 80302
01CY ATTN R. GRUBB
01CY ATTN AERONOMY LAB G. REID

DEPARTMENT OF DEFENSE CONTRACTORS

AEROSPACE CORPORATION
P. O. BOX 92957
LOS ANGELES, CA 90009
01CY ATTN I. GARFUNKEL
01CY ATTN T. SALMI
01CY ATTN V. JOSEPHSON
01CY ATTN S. BOWER
01CY ATTN N. STOCKWELL
01CY ATTN D. OLSEN

01CY ATTN SMFA FOR PWW

ANALYTICAL SYSTEMS ENGINEERING CORP
5 OLD CONCORD ROAD
BURLINGTON, MA 01803
01CY ATTN RADIO SCIENCES

BERKELEY RESEARCH ASSOCIATES, INC.
P. O. BOX 983
BERKELEY, CA 94701
01CY ATTN J. WORKMAN

BOEING COMPANY, THE
P. O. BOX 3707
SEATTLE, WA 98124
01CY ATTN G. KEISTER
01CY ATTN D. MURRAY
01CY ATTN G. HALL
01CY ATTN J. KENNEY

CALIFORNIA AT SAN DIEGO, UNIV OF
P. O. Box 6049
San Diego, CA 92106

BROWN ENGINEERING COMPANY, INC.
CUMMINGS RESEARCH PARK
HUNTSVILLE, AL 35807
01CY ATTN ROMEO A. DELIBERIS

CHARLES STARK DRAPER LABORATORY, INC.
555 TECHNOLOGY SQUARE
CAMBRIDGE, MA 02139
01CY ATTN D. B. COX
01CY ATTN J. P. GILMORE

COMPUTER SCIENCES CORPORATION
6565 ARLINGTON BLVD
FALLS CHURCH, VA 22046
01CY ATTN H. BLANK
01CY ATTN JOHN SPOOR
01CY ATTN C. NAIL

COMSAT LABORATORIES
LINTHICUM ROAD
CLARKSBURG, MD 20734
01CY ATTN G. HYDE

CORNELL UNIVERSITY
DEPARTMENT OF ELECTRICAL ENGINEERING
ITHACA, NY 14850
01CY ATTN D. T. FARLEY JR

ELECTROSPACE SYSTEMS, INC.
BOX 1359
RICHARDSON, TX 75080
01CY ATTN H. LOGSTON
01CY ATTN SECURITY (PAUL PHILLIPS)

ESL INC.
495 JAVA DRIVE
SUNNYVALE, CA 94086
01CY ATTN J. ROBERTS
01CY ATTN JAMES MARSHALL
01CY ATTN C. W. PRETTIE

FORD AEROSPACE & COMMUNICATIONS CORP
3939 FABIAN WAY
PALO ALTO, CA 94303
01CY ATTN J. T. MATTINGLEY

GENERAL ELECTRIC COMPANY
SPACE DIVISION
VALLEY FORGE SPACE CENTER
GODDARD BLVD KING OF PRUSSIA
P. O. BOX 8555
PHILADELPHIA, PA 19101
01CY ATTN M. H. BORTNER SPACE SCI LAB

GENERAL ELECTRIC COMPANY
P. O. BOX 1122
SYRACUSE, NY 13201
01CY ATTN F. REIBERT

GENERAL ELECTRIC COMPANY
TEMPO-CENTER FOR ADVANCED STUDIES
816 STATE STREET (P.O. DRAWER QQ)
SANTA BARBARA, CA 93102
01CY ATTN DASIAC
01CY ATTN DON CHANDLER
01CY ATTN TOM BARRETT
01CY ATTN TIM STEPHANS
01CY ATTN WARREN S. KNAPP
01CY ATTN WILLIAM MCNAMARA
01CY ATTN B. GAMBILL
01CY ATTN MACK STANTON

GENERAL ELECTRIC TECH SERVICES CO., INC.
HMES
COURT STREET
SYRACUSE, NY 13201
01CY ATTN G. MILLMAN

GENERAL RESEARCH CORPORATION
SANTA BARBARA DIVISION
P. O. BOX 6770
SANTA BARBARA, CA 93111
01CY ATTN JOHN ISE JR
01CY ATTN JOEL GARBARINO

GEOPHYSICAL INSTITUTE
UNIVERSITY OF ALASKA
FAIRBANKS, AK 99701
(ALL CLASS ATTN: SECURITY OFFICER)
01CY ATTN T. N. DAVIS (UNCL ONLY)
01CY ATTN NEAL BROWN (UNCL ONLY)
01CY ATTN TECHNICAL LIBRARY

GTE SYLVANIA, INC.
ELECTRONICS SYSTEMS GRP-EASTERN DIV
77 A STREET
NEEDHAM, MA 02194
01CY ATTN MARSHAL CROSS

ILLINOIS, UNIVERSITY OF
DEPARTMENT OF ELECTRICAL ENGINEERING
URBANA, IL 61803
01CY ATTN K. YEH

ILLINOIS, UNIVERSITY OF
107 COBLE HALL
801 S. WRIGHT STREET
URBANA, IL 60680
(ALL CORRES ATTN SECURITY SUPERVISOR FOR)
01CY ATTN K. YEH

INSTITUTE FOR DEFENSE ANALYSES
400 ARMY-NAVY DRIVE
ARLINGTON, VA 22202
01CY ATTN J. M. AEIN
01CY ATTN ERNEST BAUER
01CY ATTN HANS WOLFHARD
01CY ATTN JOEL BENGSTON

HSS, INC.
2 ALFRED CIRCLE
BEDFORD, MA 01730
01CY ATTN DONALD HANSEN

INTL TEL & TELEGRAPH CORPORATION
500 WASHINGTON AVENUE
NUTLEY, NJ 07110
01CY ATTN TECHNICAL LIBRARY

JAYCOR
1401 CAMINO DEL MAR
DEL MAR, CA 92014
01CY ATTN S. R. GOLDMAN

JOHNS HOPKINS UNIVERSITY
APPLIED PHYSICS LABORATORY
JOHNS HOPKINS ROAD
LAUREL, MD 20810
01CY ATTN DOCUMENT LIBRARIAN
01CY ATTN THOMAS POTEMRA
01CY ATTN JOHN DASSOULAS

LOCKHEED MISSILES & SPACE CO INC
P. O. BOX 504
SUNNYVALE, CA 94088
01CY ATTN DEPT 60-12
01CY ATTN D. R. CHURCHILL

LOCKHEED MISSILES AND SPACE CO INC
3251 HANOVER STREET
PALO ALTO, CA 94304
01CY ATTN MARTIN WALT DEPT 52-10
01CY ATTN RICHARD G. JOHNSON DEPT 52-12
01CY ATTN W. L. IMHOF DEPT 52-12

KAMAN SCIENCES CORP
P. O. BOX 7463
COLORADO SPRINGS, CO 80933
01CY ATTN T. MEAGHER

LINKABIT CORP
10453 ROSELLE
SAN DIEGO, CA 92121
01CY ATTN IRWIN JACOBS

M.I.T. LINCOLN LABORATORY
P. O. BOX 73
LEXINGTON, MA 02173
01CY ATTN DAVID M. TOWLE
01CY ATTN P. WALDRON
01CY ATTN L. LOUGHLIN
01CY ATTN D. CLARK

MARTIN MARIETTA CORP
ORLANDO DIVISION
P. O. BOX 5837
ORLANDO, FL 32805
01CY ATTN R. HEFFNER

MCDONNELL DOUGLAS CORPORATION
5301 BOLSA AVENUE
HUNTINGTON BEACH, CA 92647
01CY ATTN N. HARRIS
01CY ATTN J. MOULE
01CY ATTN GEORGE MROZ
01CY ATTN W. OLSON
01CY ATTN R. W. HALPRIN
01CY ATTN TECHNICAL LIBRARY SERVICES

MISSION RESEARCH CORPORATION
735 STATE STREET
SANTA BARBARA, CA 93101
01CY ATTN P. FISCHER
01CY ATTN W. F. CREVIER
01CY ATTN STEVEN L. GUTSCHE
01CY ATTN D. SAPPENFIELD
01CY ATTN R. BOGUSCH
01CY ATTN R. HENDRICK
01CY ATTN RALPH KILB
01CY ATTN DAVE SOWLE
01CY ATTN F. FAJEN
01CY ATTN M. SCHEIBE
01CY ATTN CONRAD L. LONGMIRE
01CY ATTN WARREN A. SCHLUETER

MITRE CORPORATION, THE
P. O. BOX 208
BEDFORD, MA 01730
01CY ATTN JOHN MORGANSTERN
01CY ATTN G. HARDING
01CY ATTN C. E. CALLAHAN

MITRE CORP
WESTGATE RESEARCH PARK
1820 DOLLY MADISON BLVD
MCLEAN, VA 22101
01CY ATTN W. HALL
01CY ATTN W. FOSTER

PACIFIC-SIERRA RESEARCH CORP
1456 CLOVERFIELD BLVD.
SANTA MONICA, CA 90404
01CY ATTN E. C. FIELD JR

PENNSYLVANIA STATE UNIVERSITY
IONOSPHERE RESEARCH LAB
318 ELECTRICAL ENGINEERING EAST
UNIVERSITY PARK, PA 16802
(NO CLASSIFIED TO THIS ADDRESS)
01CY ATTN IONOSPHERIC RESEARCH LAB

PHOTOMETRICS, INC.
442 MARRETT ROAD
LEXINGTON, MA 02173
01CY ATTN IRVING L. KOFSKY

PHYSICAL DYNAMICS INC.
P. O. BOX 3027
BELLEVUE, WA 98009
01CY ATTN E. J. FREMOUW

PHYSICAL DYNAMICS INC.
P. O. BOX 10367
OAKLAND, CA. 94610
ATTN: A. THOMSON

R & D ASSOCIATES
P. O. BOX 9695
MARINA DEL REY, CA 90291
01CY ATTN FORREST GILMORE
01CY ATTN BRYAN GABBARD
01CY ATTN WILLIAM B. WRIGHT JR
01CY ATTN ROBERT F. LELEVIER
01CY ATTN WILLIAM J. KARZAS
01CY ATTN H. ORY
01CY ATTN C. MACDONALD
01CY ATTN R. TURCO

RAND CORPORATION, THE
1700 MAIN STREET
SANTA MONICA, CA 90406
01CY ATTN CULLEN CRAIN
01CY ATTN ED BEDROZIAN

RIVERSIDE RESEARCH INSTITUTE
80 WEST END AVENUE
NEW YORK, NY 10023
01CY ATTN VINCE TRAPANI

SCIENCE APPLICATIONS, INC.
P. O. BOX 2351
LA JOLLA, CA 92038
01CY ATTN LEWIS M. LINSON
01CY ATTN DANIEL A. HAMLIN
01CY ATTN D. SACHS
01CY ATTN E. A. STRAKER
01CY ATTN CURTIS A. SMITH
01CY ATTN JACK MCDOUGALL

RAYTHEON CO.
528 BOSTON POST ROAD
SUDBURY, MA 01776
01CY ATTN BARBARA ADAMS

Science Applications, Incorporated
1710 Goodridge Drive
McLean, VA 22102
Attn: J. Cockayne

Lockheed Missile & Space Co.,Inc.
Huntsville Research & Engr. Ctr.
4800 Bradford Drive
Huntsville, Alabama 35807
Attn: Dale H. Davis

SRI INTERNATIONAL
333 RAVENSWOOD AVENUE
MENLO PARK, CA 94025
01CY ATTN DONALD NEILSON
01CY ATTN ALAN BURNS
01CY ATTN G. SMITH
01CY ATTN L. L. COBB
01CY ATTN DAVID A. JOHNSON
01CY ATTN WALTER G. CHESNUT
01CY ATTN CHARLES L. RINO
01CY ATTN WALTER JAYE
01CY ATTN M. BARON
01CY ATTN RAY L. LEADABRAND
01CY ATTN G. CARPENTER
01CY ATTN G. PRICE
01CY ATTN J. PETERSON
01CY ATTN R. HAKE, JR.
01CY ATTN V. GONZALES
01CY ATTN D. MCDANIEL

TECHNOLOGY INTERNATIONAL CORP
75 WIGGINS AVENUE
BEDFORD, MA 01730
01CY ATTN W. P. BOQUIST

TRW DEFENSE & SPACE SYS GROUP
ONE SPACE PARK
REDONDO BEACH, CA 90278
01CY ATTN R. K. PLEBUCH
01CY ATTN S. ALTSCHULER
01CY ATTN D. DEE

VISIDYNE, INC.
19 THIRD AVENUE
NORTH WEST INDUSTRIAL PARK
BURLINGTON, MA 01803
01CY ATTN CHARLES HUMPHREY
01CY ATTN J. W. CARPENTER

IONOSPHERIC MODELING DISTRIBUTION LIST
UNCLASSIFIED ONLY

PLEASE DISTRIBUTE ONE COPY TO EACH OF THE FOLLOWING PEOPLE:

ADVANCED RESEARCH PROJECTS AGENCY (ARPA)
STRATEGIC TECHNOLOGY OFFICE
ARLINGTON, VIRGINIA

CAPT. DONALD M. LEVINE

NAVAL RESEARCH LABORATORY
WASHINGTON, D.C. 20375

DR. P. MANGE
DR. R. MEIER
DR. E. SZUSZCZEWICZ - CODE 4127

DR. J. GOODMAN - CODE 7560

SCIENCE APPLICATIONS, INC.
1250 PROSPECT PLAZA
LA JOLLA, CALIFORNIA 92037

DR. D. A. HAMLIN
DR. L. LINSON
DR. D. SACHS

DIRECTOR OF SPACE AND ENVIRONMENTAL LABORATORY
NOAA
BOULDER, COLORADO 80302

DR. A. GLENN JEAN
DR. G. W. ADAMS
DR. D. N. ANDERSON
DR. K. DAVIES
DR. R. F. DONNELLY

A. F. GEOPHYSICS LABORATORY
L. G. HANSOM FIELD
BEDFORD, MASS. 01730

DR. T. ELKINS
DR. W. SWIDER
MRS. R. SAGALYN
DR. J. M. FORBES
DR. T. J. KENESHEA
DR. J. AARONS

OFFICE OF NAVAL RESEARCH
800 NORTH QUINCY STREET
ARLINGTON, VIRGINIA 22217

DR. H. MULLANEY

COMMANDER
NAVAL ELECTRONICS LABORATORY CENTER
SAN DIEGO, CALIFORNIA 92152

DR. M. BLEIWEISS
DR. I. ROTHMULLER
DR. V. HILDEBRAND
MR. R. ROSE

U. S. ARMY ABERDEEN RESEARCH AND DEVELOPMENT CENTER
BALLISTIC RESEARCH LABORATORY
ABERDEEN, MARYLAND

DR. J. HEIMERL

COMMANDER
NAVAL AIR SYSTEMS COMMAND
DEPARTMENT OF THE NAVY
WASHINGTON, D.C. 20360

DR. T. CZUBA

HARVARD UNIVERSITY
HARVARD SQUARE
CAMBRIDGE, MASS. 02138

DR. M. B. MCELROY
DR. R. LINDZEN

PENNSYLVANIA STATE UNIVERSITY
UNIVERSITY PARK, PENNSYLVANIA 16802

DR. J. S. NISBET
DR. P. R. ROHRBAUGH
DR. D. E. BARAN
DR. L. A. CARPENTER
DR. M. LEE
DR. R. DIVANY
DR. P. BENNETT
DR. E. KLEVANS

UNIVERSITY OF CALIFORNIA, LOS ANGELES
405 HILLGARD AVENUE
LOS ANGELES, CALIFORNIA 90024

DR. F. V. CORONITI
DR. C. KENNEL

UNIVERSITY OF CALIFORNIA, BERKELEY
BERKELEY, CALIFORNIA 94720

DR. M. HUDSON

UTAH STATE UNIVERSITY
4TH N. AND 8TH STREETS
LOGAN, UTAH 84322

DR. P. M. BANKS
DR. R. HARRIS
DR. V. PETERSON
DR. R. MEGILL
DR. K. BAKER

CORNELL UNIVERSITY
ITHACA, NEW YORK 14850

DR. W. E. SWARTZ
DR. R. SUDAN
DR. D. FARLEY
DR. M. KELLEY

NASA
GODDARD SPACE FLIGHT CENTER
GREENBELT, MARYLAND 20771

DR. S. CHANDRA
DR. K. MAEDO

PRINCETON UNIVERSITY
PLASMA PHYSICS LABORATORY
PRINCETON, NEW JERSEY 08540

DR. F. PERKINS
DR. E. FRIEMAN

INSTITUTE FOR DEFENSE ANALYSIS
400 ARMY/NAVY DRIVE
ARLINGTON, VIRGINIA 22202

DR. E. BAUER

UNIVERSITY OF MARYLAND
COLLEGE PARK, MD 20742
DR. K. PAPADOPOULOS
DR. E. OTT

UNIVERSITY OF PITTSBURGH
PITTSBURGH, PA. 15213

DR. N. ZABUSKY
DR. M. BIONDI

DEFENSE DOCUMENTATION CENTER
CAMERON STATION
ALEXANDRIA, VA. 22314

(12 COPIES IF OPEN PUBLICATION
OTHERWISE 2 COPIES) 12CY ATTN TC

UNIVERSITY OF CALIFORNIA
LOS ALAMOS SCIENTIFIC LABORATORY
J-10, MS-664
LOS ALAMOS, NEW MEXICO 87545

M. PONGRATZ
D. SIMONS
G. BARASCH
L. DUNCAN

Massachusetts Institute of Technology
Plasma Fusion Center
Library, NW16-262
Cambridge, MA 02139

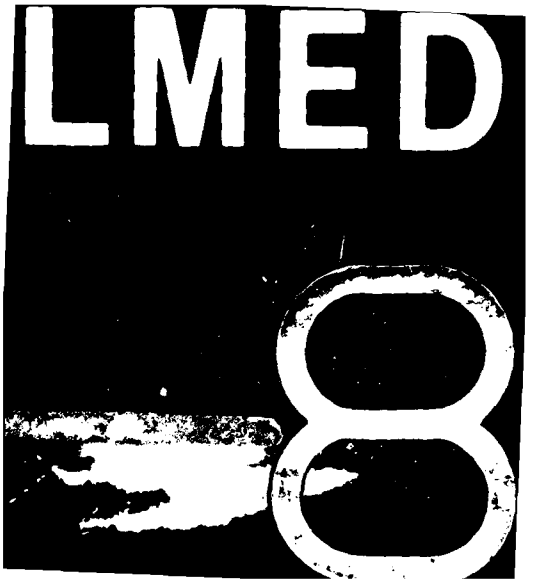
LMED
8